Geometry-Based Statistical Modeling of Non-WSSUS Mobile-to-Mobile Rayleigh Fading Channels

Carlos A. Gutiérrez, *Member, IEEE,* José T. Gutiérrez-Mena, *Student Member, IEEE,*
José M. Luna-Rivera, Daniel U. Campos-Delgado, *Senior Member, IEEE*,
Ramiro Velázquez, and Matthias Pätzold, *Senior Member, IEEE*

***Abstract*—In this paper, we present a novel geometry-based statistical model (GBSM) for small-scale non-wide-sense stationary uncorrelated scattering (non-WSSUS) mobile-to-mobile (M2M) Rayleigh fading channels. The proposed model builds on the principles of plane wave propagation (PWP) to capture the temporal evolution of the propagation delay and Doppler shift of the received multipath signal. This is different from existing non-WSSUS geometry-based statistical channel models, which are based on a spherical wave propagation (SWP) approach, that in spite of being more realistic, is more mathematically intricate. By considering an arbitrary geometrical configuration of the propagation area, we derive general expressions for the most important statistical quantities of nonstationary channels, such as the first-order probability density functions (PDFs) of the envelope and phase, the four-dimensional (4D) time-frequency correlation function (TF-CF), local scattering function (LSF), and time-frequency (TF) dependent delay and Doppler profiles. We also present an approximate closed-form expression of the channel's 4D TF-CF for the particular case of the geometrical one-ring scattering model. The obtained results provide new theoretical insights into the correlation and spectral properties of non-WSSUS M2M Rayleigh fading channels.**

***Index Terms*—Fading channels, mobile-to-mobile communications, nonstationary processes, radiowave propagation, non-wide-sense stationary uncorrelated scattering (non-WSSUS) channels.**

I. Introduction

THE characterization of nonstationary time-frequency (TF) dispersive multipath fading channels is a topic of research that is receiving increasing attention due to the emergence of novel mobile communication systems that are conceived to operate under rapidly changing propagation conditions. Examples of such systems include high-speed railway communication systems [1], fourth (4G) [2] and fifth generation (5G) [3] cellular networks for on-the-road communications, and dedicated short-range communication (DSRC) systems for wireless access in vehicular environments [4]. Measured data collected for these systems show that the wide-sense stationary uncorrelated scattering (WSSUS) assumption, often invoked to characterize TF dispersive multipath fading channels, is only valid over limited and rather short time and frequency intervals [5], [6]. Aiming to analytically characterize such empirical findings, several different geometry-based statistical models (GBSMs) for non-WSSUS mobile-to-mobile (M2M) fading channels have been proposed in recent years, e.g., in [7]–[9]. To the best of the authors' knowledge, all these models have been developed following a spherical wave propagation (SWP) approach. In the SWP framework, the angle of departure (AOD) and angle of arrival (AOA) of the received electromagnetic waves are modeled as time-varying quantities determined by the instantaneous relative position between the wave source (transmitter antennas or interfering objects, IOs) and the observer (IOs or receiver antennas) [7]. On the other hand, the path length of the received waves are modeled by the Euclidean distance between source and observer.

The SWP approach provides a realistic description of the physical process of radiowave propagation, but it renders the mathematical analysis of the channel's statistics a cumbersome task [7], [9]. To facilitate such task, we present in this paper a novel GBSM for nonstationary TF dispersive M2M Rayleigh fading channels that builds instead on the principles of plane wave propagation (PWP). The proposed model is particularly well-suited for analyzing the channel's nonstationarities arising at a small-scale level due to the time-varying nature of the propagation delays. The geometry-based statistical modeling approach and the PWP model are a well-known tandem for the characterization of TF dispersive fixed-to-mobile (F2M) and M2M fading channels. However, the existing geometrical PWP models for F2M and M2M Rayleigh fading channels have been formulated assuming time-invariant propagation delays to enforce the fulfillment of the WSSUS condition (see, e.g., [10]–[12]). For this reason, they do not provide insights into the propagation delays' temporal evolution. By contrast, our model characterizes the aforementioned evolution as an inherent process to the propagation of radiowaves.

On the grounds of the proposed model, we derive general expressions for important statistical quantities of nonstationary channels, such as the first-order probability density functions (PDFs) of the envelope and phase, the four-dimensional (4D)

Manuscript submitted April 19, 2016, revised December 9, 2016, April 18, 2017, and June 4, 2017, accepted August 5, 2017.

C. A. Gutiérrez, J. T. Gutiérrez-Mena, J. M. Luna-Rivera, and D. U. Campos-Delgado are with the Faculty of Science, Universidad Autónoma de San Luis Potosí, Av. Salvador Nava Mtz. s/n, Zona Universitaria, San Luis Potosi 78290, Mexico (e-mails: {cagutierrez, j.g.gutierrez}@ieee.org, {mlr, ducd}@fciencias.uaslp.mx).

R. Velázquez is with the Faculty of Engineering, Universidad Panamericana, Josemaría Escrivá de Balaguer No. 101, Aguascalientes 20120, Mexico (e-mail: rvelazquez@up.edu.mx).

M. Pätzold is with the Department of Information and Communication Technology, Faculty of Engineering and Science, University of Agder, P.O. Box 509, 4898 Grimstad, Norway (e-mail: matthias.paetzold@uia.no).

TF correlation function (TF-CF), local scattering function (LSF), and TF-dependent delay and Doppler profiles. In addition, we derive a novel closed-form expression for the channel 4D TF-CF for the particular case of the geometrical one-ring scattering model. This scattering model has widely been employed as a reference model to analyze the correlation properties of multipath F2M and M2M fading channels assuming single interactions with IOs [13]. A related model, which is more representative for vehicular communication scenarios, is the geometrical two-rings scattering model [14]. The analysis of the two-rings model is not addressed in this paper, as the double interaction with IOs requires modifications of the modeling framework presented herein. However, the extension has recently been addressed in [15].

In spite of recent advances in the empirical modeling of nonstationary channels, there are currently no measurements available that allow for a direct comparison between our theoretical results and empirical data. However, even though the proposed channel model is yet to be validated empirically, it gives theoretical insights into some characteristics of nonstationary M2M fading channels that have been observed empirically, such as those discussed in [16], where it has been noted that the channel's nonstationarities are more severe in the time domain than in the frequency domain.

The remainder of the paper is organized as follows: A generic impulse response model for small-scale TF dispersive M2M channels is presented in Section II. Using this model as a baseline, we review in Section III the basics of the SWP channel modeling approach. Our proposal for the geometrical PWP modeling of non-WSSUS M2M Rayleigh fading channels is introduced in Section IV. The first-order statistics, as well as the correlation and spectral properties of the proposed channel model are analyzed in Section V by considering an arbitrary geometrical configuration of the propagation scenario. In Section VI, we analyze the channel model's correlation and spectral properties for the particular case of the geometrical one-ring scattering model. Finally, our conclusions are summarized in Section VII.

Notation: The complex conjugate and the absolute value operators are denoted by $(\cdot)^*$ and $|\cdot|$, respectively. Vectors are written in bold face. The transpose operator is denoted by $(\cdot)^\dagger$, $\arg\{\cdot\}$ indicates the angle of a two-dimensional (2D) vector, $\|\cdot\|$ stands for the Euclidean norm, and the scalar product between two vectors $\mathbf{z}_1$ and $\mathbf{z}_2$ is represented as $\langle \mathbf{z}_1, \mathbf{z}_2 \rangle$. The operator $\mathcal{E}\{\cdot\}$ designates the statistical expectation. The sets of real numbers and positive real numbers are denoted by $\mathbb{R}$ and $\mathbb{R}^+$, respectively.

II. Mathematical Model of TF Dispersive M2M Rayleigh Fading Channels

The small-scale TF-dispersive M2M Rayleigh fading channel is characterized in this paper as follows: Suppose that the transmitted signal reaches the receive antenna by single interactions with $\mathcal{L}$ fixed (non-moving) IOs. Suppose also that the transmitted and the received signals are linearly polarized, and assume that the far-field condition holds. Then, for a finite observation time window of length T_0, the channel impulse response (CIR) at time t due to an impulse applied τ seconds in the past can be characterized in the equivalent baseband by the superposition of $\mathcal{L}$ electromagnetic waves as follows

$$h(t;\tau) \triangleq \sum_{\ell=1}^{\mathcal{L}} g_\ell \exp\left\{ j\left[\theta_\ell + \vartheta_\ell^T(t) + \vartheta_\ell^R(t)\right]\right\} \times \delta\left(\tau - \tau_\ell(t)\right) \cdot \Omega_{T_0}(t - t_0). \quad (1)$$

In the previous equation, $j^2 = -1$; g_ℓ and θ_ℓ stand for the attenuation and phase shift introduced by the interaction with the ℓth IO, respectively; $\vartheta_\ell^T(t)$ and $\vartheta_\ell^R(t)$ account for the rotation of the wave's phase due to the distance traveled at a given time instant t ($\vartheta_\ell^T(t)$ is associated with the path from the transmit antenna to the ℓth IO, and $\vartheta_\ell^R(t)$ with the path from the ℓth IO to the receive antenna); $\delta(\cdot)$ is the Dirac delta function; and $\tau_\ell(t)$ stands for the time-varying propagation delay of the ℓth received wave. The windowing function $\Omega_{T_0}(t - t_0)$ is defined as

$$\Omega_{T_0}(t - t_0) \triangleq \begin{cases} 1, & t_0 \le t \le t_0 + T_0 \\ 0, & \text{otherwise} \end{cases} \quad (2)$$

where t_0 indicates the time instant at which the transmitter starts to communicate with the receiver.

The gains g_ℓ and phases θ_ℓ of the multipath components in (1) are in general functions of time that depend of the IOs' electromagnetic properties. However, for the wave propagation over local areas (spanning a few tens of wavelengths), these parameters can be modeled as constant quantities, and their dependence on the IO's electromagnetic properties can be obviated if they are characterized as random variables (r.v.) (see, e.g., [17], [18]). In this paper, we follow this latter approach, since we are primarily interested in the small-scale modeling of M2M fading channels. On the other hand, the length of the CIR $h(t;\tau)$ in (1) with respect to time t may be infinitely large, such that $T_0 \to \infty$. However, if a large observation time interval is considered, then the parameters of $h(t;\tau)$ should account also for the channel's large-scale dynamics. Thus, for the purposes of this paper, we will assume that T_0 is small enough as to neglect the channel's large-scale variations (e.g., path loss, shadowing due to obstructions by large IOs, and those caused by the appearance and disappearance of IOs). For example, if we consider a DSRC system operating in the 5.9 GHz band [4], and a mobile station moving with a speed of 100 km/h, then we can set $T_0 = 60$ ms, as this is the time that the mobile station would take to transit through a local area of about 30 wavelengths. The mathematical model of $h(t;\tau)$ presented in (1) is quite general, and it can be parameterized to account for almost any form of interaction with IOs, except those that produce group delay distortion, since we are not considering the time-varying nature of the gains g_ℓ, nor their dependence on the IOs' electrical properties.

III. Overview of the Geometrical SWP Channel Modeling Approach

The definition of $h(t;\tau)$ given by (1) is valid for both SWP and PWP. The difference between these two modeling frameworks lies essentially in the way in which the time-varying parameters $\vartheta_\ell^T(t)$, $\vartheta_\ell^R(t)$, and $\tau_\ell(t)$ are defined. In

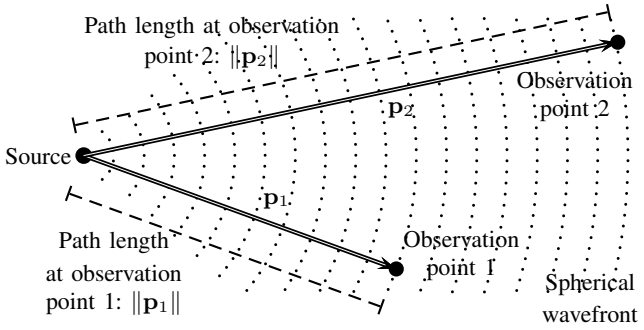

Fig. 1. Geometry of the propagation of a spherical wavefront.

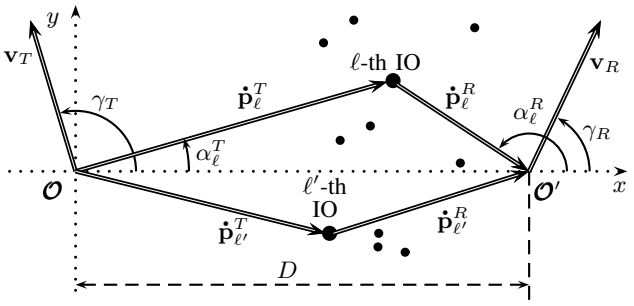

Fig. 2. The reference 2D propagation scenario at time $t_0 = 0$.

the SWP framework, $\vartheta_\ell^T(t)$, $\vartheta_\ell^R(t)$, and $\tau_\ell(t)$ are modeled by assuming that the transmitted waves propagate radially outward the source [19, Sec. 1.7.2]. Thereby, the resulting spherical wavefront reaches a given observation point by traveling over a path with a length equal to the Euclidean distance between the source and the observer. This propagation mechanism is illustrated in Fig. 1, where vector $\mathbf{p}_i$ indicates the position of the ith observer relative to the source location. In this context, the time-varying phases $\vartheta_\ell^T(t)$ and $\vartheta_\ell^R(t)$, and the propagation delay $\tau_\ell(t)$ in (1), can be defined as [7]–[9]:

$$\vartheta_\ell^T(t) \triangleq \kappa_0 \|\mathbf{p}_\ell^T(t)\| \quad (3)$$

$$\vartheta_\ell^R(t) \triangleq \kappa_0 \|\mathbf{p}_\ell^R(t)\| \quad (4)$$

$$\tau_\ell(t) \triangleq \frac{\|\mathbf{p}_\ell^T(t)\| + \|\mathbf{p}_\ell^R(t)\|}{\mathcal{C}} \quad (5)$$

where $\kappa_0 \triangleq 2\pi/\lambda$ is the phase constant (wavenumber), λ is the transmitted signal's wavelength; $\mathcal{C}$ stands for the speed of light; the vector $\mathbf{p}_\ell^T(t)$ indicates the position of the ℓth IO relative to the transmitter at time t; and $\mathbf{p}_\ell^R(t)$ describes the position of the receiver as seen from the ℓth IO also at time t. These two vectors are time varying, since the position of the transmitter and the receiver is changing over time. Furthermore, if the IOs are randomly located in the propagation area, then $\mathbf{p}_\ell^T(t)$ and $\mathbf{p}_\ell^R(t)$ are stochastic vectors, and therefore $\vartheta_\ell^T(t)$, $\vartheta_\ell^R(t)$, and $\tau_\ell(t)$ are stochastic processes, as they are modeled by functions of time with random parameters. In our modeling framework, once the random values of the time-varying phases and propagation delays are drawn, their evolution in time is deterministic, as propagation physics would predict.

The position vectors $\mathbf{p}_\ell^T(t)$ and $\mathbf{p}_\ell^R(t)$ can be characterized with respect to a given geometrical configuration of the propagation scenario, such as the one shown in Fig. 2. In this figure, the IOs are represented by black dots. The origin of the coordinate system is given by the location of the transmit antenna at time t_0 (i.e., at the time at which the transmitter starts to communication with the receiver), and is denoted by $\mathcal{O}$. On the other hand, $\mathcal{O}'$ designates the location of the receive antenna also at time t_0. Without loss of generality, we will henceforth assume that $t_0 = 0$. The distance between the fixed reference points $\mathcal{O}$ and $\mathcal{O}'$ is denoted by D.

Throughout the paper, we assume that the transmitter and the receiver move at constant speeds ν_T and ν_R along linear trajectories described by the angles γ_T and γ_R. Thereby, we can write the velocity vectors of the transmitter and the receiver as:

$$\mathbf{v}_T = \nu_T \left[\cos(\gamma_T), \sin(\gamma_T)\right]^\dagger \quad (6a)$$

$$\mathbf{v}_R = \nu_R \left[\cos(\gamma_R), \sin(\gamma_R)\right]^\dagger. \quad (6b)$$

Thus, regardless of the IOs' location, we have:

$$\mathbf{p}_\ell^T(t) = \dot{\mathbf{p}}_\ell^T - t \cdot \mathbf{v}_T \quad (7a)$$

$$\mathbf{p}_\ell^R(t) = \dot{\mathbf{p}}_\ell^R + t \cdot \mathbf{v}_R \quad (7b)$$

for $t \geq 0$, where

$$\dot{\mathbf{p}}_\ell^T = d_\ell^T \left[\cos(\alpha_\ell^T), \sin(\alpha_\ell^T)\right]^\dagger \quad (8a)$$

$$\dot{\mathbf{p}}_\ell^R = d_\ell^R \left[\cos(\pi + \alpha_\ell^R), \sin(\pi + \alpha_\ell^R)\right]^\dagger. \quad (8b)$$

In (8), d_ℓ^T and d_ℓ^R stand for the Euclidean distances between the ℓth IO and the reference points $\mathcal{O}$ and $\mathcal{O}'$, respectively. In turn, the angles α_ℓ^T and α_ℓ^R indicate the direction to the ℓth IO from $\mathcal{O}$ and $\mathcal{O}'$, respectively (see Fig. 2).

Substituting (7) into (3)–(5), we find that:

$$\vartheta_\ell^T(t) = \kappa_0\, d_\ell^T - t 2\pi f_{\max}^T \cos(\phi_\ell^T(t) - \gamma_T) \quad (9)$$

$$\vartheta_\ell^R(t) = \kappa_0\, d_\ell^R - t 2\pi f_{\max}^R \cos(\phi_\ell^R(t) - \gamma_R) \quad (10)$$

$$\tau_\ell(t) = \frac{d_\ell^T + d_\ell^R}{\mathcal{C}} - t\frac{f_{\ell,D}^{SW}(t)}{f_c} \quad (11)$$

where

$$\phi_\ell^T(t) = \arg\{\mathbf{p}_\ell^T(t)\} \quad (12a)$$

$$\phi_\ell^R(t) = \pi + \arg\{\mathbf{p}_\ell^R(t)\} \quad (12b)$$

are the time-varying AOD and AOA of the ℓth received wave, respectively, $f_c = \mathcal{C}/\lambda$ is the carrier frequency, and

$$f_{D,\ell}^{SW}(t) = f_{\max}^T \cos(\phi_\ell^T(t) - \gamma_T) + f_{\max}^R \cos(\phi_\ell^R(t) - \gamma_R). \quad (13)$$

In (13), $f_{\max}^T \triangleq \nu_T/\lambda$ and $f_{\max}^R \triangleq \nu_R/\lambda$ are the maximum Doppler shifts due to the movement of the transmitter and the receiver, respectively. Using (9)–(13), we can rearrange (1) as

$$h(t;\tau) = \sum_{\ell=1}^{\mathcal{L}} g_\ell \exp\left\{j\left[\theta_\ell + 2\pi f_c \tau_\ell(t)\right]\right\} \times \delta\left(\tau - \tau_\ell(t)\right) \cdot \Omega_{T_0}(t). \quad (14)$$

This alternative form of $h(t;\tau)$ highlights the fact that the

time-varying parameters $\vartheta_\ell^T(t)$, $\vartheta_\ell^R(t)$, and $\tau_\ell(t)$ are modeled by considering a common path length (cf. [20, Eq. 14.1–5]).

IV. The Proposed Geometrical PWP Model for Non-WSSUS M2M Channels

A distinctive characteristic of the geometrical SWP channel models is that the AODs and AOAs of the received waves are time-varying quantities, as shown by (12). This feature makes the SWP models well-suited for characterizing nonstationary channels, but renders the mathematical analysis of important channel statistics, such as the 4D TF-CF, a cumbersome task. A well-known solution to simplify calculations is to consider a plane wave approximation of spherical waves. This approximation involves assuming that distances are sufficiently large that wavefronts at relevant positions can be considered as planar. Thereby, the AODs/AOAs remain constant for any observation point along the wavefront [19, Sec. 1.7.3]. This simplification is valid in the context of short-range vehicular communication for propagation over small local areas, provided that the far-field condition holds [21].[1]

In the PWP framework, the path length of a traveling wave is approximated by the scalar projection $\langle \mathbf{p}, \mathbf{u} \rangle$, where $\mathbf{p}$ describes the observer's position relative to the source's location, and $\mathbf{u}$ is a unit vector that points at the direction of propagation, as illustrated in Fig. 3. Note that this scalar projection is a mathematical description of the parallel rays representation of a traveling planar wavefront [19, Sec. 1.7.3]. With this in mind, we define the phase shifts $\vartheta_\ell^T(t)$ and $\vartheta_\ell^R(t)$, and the propagation delay $\tau_\ell(t)$ as:

$$\vartheta_\ell^T(t) \triangleq \kappa_0 \langle \mathbf{p}_\ell^T(t), \mathbf{u}_\ell^T \rangle \quad (15)$$

$$\vartheta_\ell^R(t) \triangleq \kappa_0 \langle \mathbf{p}_\ell^R(t), \mathbf{u}_\ell^R \rangle \quad (16)$$

$$\tau_\ell(t) \triangleq \frac{\langle \mathbf{p}_\ell^T(t), \mathbf{u}_\ell^T \rangle + \langle \mathbf{p}_\ell^R(t), \mathbf{u}_\ell^R \rangle}{\mathcal{C}} \quad (17)$$

where $\mathbf{u}_\ell^T$ and $\mathbf{u}_\ell^R$ are dimensionless unit vectors pointing in the direction of propagation of the ℓth received plane wave on transmission and after interacting with the IO, respectively. To ensure consistency, we assume that the angle between $\mathbf{p}_\ell^T(t)$ and $\mathbf{u}_\ell^T$, as well as that between $\mathbf{p}_\ell^R(t)$ and $\mathbf{u}_\ell^R$, is greater than $-\pi/2$ and smaller than $+\pi/2$. The unit vectors $\mathbf{u}_\ell^T$ and $\mathbf{u}_\ell^R$ can be written in terms of the AOD ϕ_ℓ^T and AOA ϕ_ℓ^R as:

$$\mathbf{u}_\ell^T = \left[\cos(\phi_\ell^T), \sin(\phi_\ell^T)\right]^\dagger \quad (18a)$$

$$\mathbf{u}_\ell^R = \left[\cos(\pi + \phi_\ell^R), \sin(\pi + \phi_\ell^R)\right]^\dagger. \quad (18b)$$

Note that in the context of the PWP, the AODs ϕ_ℓ^T and AOAs ϕ_ℓ^R are time-invariant quantities, as they are not determined by the relative position between the source and the observer.

Assuming that the unit vectors $\mathbf{u}_\ell^T$ and $\mathbf{u}_\ell^R$ are collinear with $\dot{\mathbf{p}}_\ell^T$ and $\dot{\mathbf{p}}_\ell^R$, respectively, in such a way that

$$\phi_\ell^T = \alpha_\ell^T \quad (19a)$$

$$\phi_\ell^R = \alpha_\ell^R \quad (19b)$$

[1]The far-field condition varies from one antenna type to another. However, as a rule of thumb, this condition is said to be fulfilled if the wave source and the observer are separated by a distance that produces a phase error between the spherical and the plane wave model not larger than 22.5° [19]. For electrically large antennas, the far-field region starts at a distance of $2a^2/\lambda$ from the source, where a is the largest dimension of the antenna.

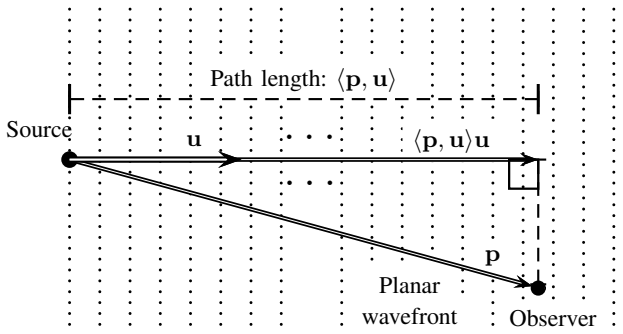

Fig. 3. Geometry of the propagation of a planar wavefront.

we find from the definitions in (6), (7), and (15)–(18) that:

$$\vartheta_\ell^T(t) = \kappa_0 \, d_\ell^T - t 2\pi f_{\max}^T \cos(\phi_\ell^T - \gamma_T) \quad (20)$$

$$\vartheta_\ell^R(t) = \kappa_0 \, d_\ell^R - t 2\pi f_{\max}^R \cos(\phi_\ell^R - \gamma_R) \quad (21)$$

$$\tau_\ell(t) = \frac{d_\ell^T + d_\ell^R}{\mathcal{C}} - t \frac{f_{D,\ell}^{PW}}{f_c} \quad (22)$$

where

$$f_{D,\ell}^{PW} = f_{\max}^T \cos(\phi_\ell^T - \gamma_T) + f_{\max}^R \cos(\phi_\ell^R - \gamma_R). \quad (23)$$

It is important to point out that the Doppler frequencies $f_{D,\ell}^{PW}$ in (23) differ from their SWP counterparts in (13) only by the time-invariant nature of the AODs and AOAs. While subtle, this difference simplifies considerably the mathematical analysis of the correlation and spectral properties of non-WSSUS M2M fading channels. Note that if the IOs are randomly located in the propagation area, then the Doppler frequencies $f_{D,\ell}^{PW}$ are random variables. They are therefore more mathematically tractable than the Doppler frequencies $f_{D,\ell}^{SW}(t)$ in (13), which are stochastic processes.

The generic model of the CIR $h(t;\tau)$ given by (1) and (20)–(22) (or in general, by (1) and (15)–(17)) constitutes our proposal for the characterization of non-WSSUS M2M channels. In spite of the model's simplicity and intuitive formulation, we are not aware of any previous work proposing an equivalent representation of TF-dispersive M2M fading channels. A review of the literature shows that the existing geometrical PWP models for TF dispersive F2M and M2M channels are based on a mathematical model of the CIR that can also be written as in (1). However, the time-varying phase shifts $\vartheta_\ell^T(t)$ and $\vartheta_\ell^R(t)$, and the propagation delay $\tau_\ell(t)$, are modeled in the literature as (e.g., see [10]–[12]):

$$\vartheta_\ell^T(t) = \kappa_0 \, d_\ell^T - t 2\pi f_{\max}^T \cos(\phi_\ell^T - \gamma_T) \quad (24)$$

$$\vartheta_\ell^R(t) = \kappa_0 \, d_\ell^R - t 2\pi f_{\max}^R \cos(\phi_\ell^R - \gamma_R) \quad (25)$$

$$\tau_\ell(t) = \tau_\ell = \frac{d_\ell^T + d_\ell^R}{\mathcal{C}}. \quad (26)$$

Even though the phases in (24) and (25) are the same as those in (20) and (21), the propagation delay is defined in (26) as a time-invariant quantity τ_ℓ. This is clearly opposite to our definition of $\tau_\ell(t)$ given by (22). The assumption of time-invariant delays is necessary to fulfill the WSSUS condition. Nevertheless, this assumption imposes an important limitation,

as it does not allow characterizing the delay drift of non-WSSUS channels that has been observed from measurements [6], [16]. Moreover, in spite of the fact that the propagation delay is characterized in (26) with respect to a time-independent path length, the phase shifts $\vartheta_\ell^T(t)$ and $\vartheta_\ell^R(t)$ are modeled in (24) and (25) by considering plane waves that travel over paths whose lengths vary in time (as required to incorporate the Doppler shift effect into the channel model). This observation unveils an important inconsistency in the formulation of (24)–(26) that does not allow expressing the resulting CIR model as in (14). Note that to be consistent, $\vartheta_\ell^T(t)$, $\vartheta_\ell^R(t)$, and $\tau_\ell(t)$ should be modeled with respect to a common (time-varying or time-invariant) path length, as mentioned in Section III. By contrast, the CIR in (1) can be simplified to (14) if $\vartheta_\ell^T(t)$, $\vartheta_\ell^R(t)$, and $\tau_\ell(t)$ are modeled according to (20)–(23).

The modeling framework proposed in this section can easily be extended to the case of three-dimensional propagation environments, multiple interactions with IOs, and multipath channels with moving IOs. This framework can also be extended to incorporate the effects of acceleration and non-linear motion trajectories of the mobile stations. Recent advances in that regard can be found in [15] and [22].

V. Statistical Properties of the Proposed GBSM for Non-WSSUS M2M Channels

A. Considerations

In this section, we analyze the PDFs of the envelope and phase, the 4D TF-CF, LSF, and TF-dependent delay and Doppler profiles of the transfer function $H(t;f) \triangleq \int_{-\infty}^{\infty} h(t;\tau)\exp\{-j2\pi f\tau\}\,\mathrm{d}\tau$ of the proposed channel model. For that purpose, we will make the following considerations:

- The gains g_ℓ in (1) are positive r.v. They are not necessarily identically distributed, but are given in such a way that the sum of their average powers is a constant quantity σ_h^2 equal to the average power of the received multipath signal, i.e.,
$$\sum_{\ell=1}^{\mathcal{L}} \mathcal{E}\{|g_\ell|^2\} \;=\; \mathcal{E}\{|H(t;f)|^2\} \;=\; \sigma_h^2. \tag{27}$$
- The phases θ_ℓ are r.v. uniformly distributed in $[-\pi,\pi)$.
- The distances d_ℓ^T and d_ℓ^R in (8) are positive-valued functions of the AODs ϕ_ℓ^T and AOAs ϕ_ℓ^R, i.e.:
$$d_\ell^T \;=\; \mathcal{G}_T(\phi_\ell^T), \qquad \mathcal{G}_T : [-\pi,\pi) \longmapsto \mathbb{R}^+ \tag{28a}$$
$$d_\ell^R \;=\; \mathcal{G}_R(\phi_\ell^R), \qquad \mathcal{G}_R : [-\pi,\pi) \longmapsto \mathbb{R}^+. \tag{28b}$$
- The AODs ϕ_ℓ^T and AOAs ϕ_ℓ^R are circular symmetric r.v. characterized by PDFs $p_\phi^T(\phi)$, and $p_\phi^R(\phi)$, respectively.
- Only one side of the radio link is affected by local interactions with IOs. If the interactions occur on the receiver side, then the AODs ϕ_ℓ^T and the AOAs ϕ_ℓ^R are related by the non-linear transformation
$$\phi_\ell^T \;=\; \arctan\left(\frac{d_\ell^R\sin(\phi_\ell^R)}{D + d_\ell^R\cos(\phi_\ell^R)}\right), \quad \forall \ell. \tag{29}$$
Note that $\dot{\mathbf{p}}_\ell^T = [D,0]^\dagger - \dot{\mathbf{p}}_\ell^R$. Therefore, we have $\phi_\ell^T = \arg\{\dot{\mathbf{p}}_\ell^T\} = \arg\{[D,0]^\dagger - \dot{\mathbf{p}}_\ell^R\}$. On the other hand, if the interactions with IOs occur on the transmitter side, then ϕ_ℓ^T and ϕ_ℓ^R are related by
$$\phi_\ell^R \;=\; \pi + \arctan\left(\frac{d_\ell^T\sin(\phi_\ell^T)}{d_\ell^T\cos(\phi_\ell^T) - D}\right), \quad \forall \ell. \tag{30}$$
Note that $\phi_\ell^R = \arg\{\dot{\mathbf{p}}_\ell^R\} = \arg\{[D,0]^\dagger - \dot{\mathbf{p}}_\ell^T\}$.
- The gains g_ℓ, phases θ_ℓ, and AODs ϕ_ℓ^T form a set of $3\times\mathcal{L}$ statistically independent r.v.

B. Distributions of the Envelope and Phase

Substituting (14) into the definition of $H(t;f)$, we find that
$$H(t;f) = \Omega_{T_0}(t)\sum_{\ell=1}^{\mathcal{L}} g_\ell \exp\left\{j\big[\theta_\ell + 2\pi\tau_\ell(t)[f_c - f]\big]\right\}. \tag{31}$$
Under the conditions stated in the previous subsection, one can easily verify that the mean value and the variance of $H(t;f)$ are constant quantities equal to zero and σ_h^2, respectively. In addition, following a similar procedure as the one applied in [23] to investigating the envelope distribution of sum-of-cisoids (SOC) processes of Class VIII, it can be shown that the first-order PDF $p_\zeta(z;t,f)$ of the envelope $\zeta(t,f) \triangleq |H(t;f)|$ of $H(t;f)$ is equal to
$$p_\zeta(z;t,f) \;=\; (2\pi)^2 z \int_0^\infty \left[\prod_{\ell=1}^{\mathcal{L}} \int_0^\infty p_\ell^g(y_\ell) J_0(2\pi x y_\ell)\,\mathrm{d}y_\ell\right] \times J_0(2\pi z x) x\,\mathrm{d}x, \quad z \geq 0 \tag{32}$$
for $t \in [0,T_0]$, and $f \in \mathbb{R}$. where $p_\ell^g(\cdot)$ is the PDF of the ℓth random gain g_ℓ, and $J_0(\cdot)$ is the Bessel function of the first kind and zero order. In turn, the PDF $p_\psi(\varphi;t,f)$ of the phase $\psi(t,f) \triangleq \arg\{H(t;f)\}$ is found to be given as
$$p_\psi(\varphi;t,f) \;=\; \frac{1}{2\pi}, \quad \varphi \in [-\pi,\pi) \tag{33}$$
for $t \in [0,T_0]$, and $f \in \mathbb{R}$.

Equations (32) and (33) show that the envelope $\zeta(t,f)$ and phase $\psi(t,f)$ of the proposed channel model are first-order stationary random processes, as their corresponding PDFs do not change over time and frequency. It is important to stress that this characteristic does not imply that the channel transfer function $H(t;f)$ is a WSS random process, as we also need information about the 4D TF-CF to reach that conclusion. We can further observe from (33) that the phase $\psi(t,f)$ is modeled by a uniform circular distribution, regardless of the number of multipath components $\mathcal{L}$. On the other hand, for large values of $\mathcal{L}$ (infinitely large, in theory), the central limit theorem guarantees the convergence of $p_\zeta(z;t,f)$ to the Rayleigh PDF with parameter $\sigma_h^2/2$. The rate of convergence will vary depending on the form of the PDFs of the gains g_ℓ. However, if the gains follow a Rayleigh distribution, then (32) can be simplified to (see Appendix A)
$$p_\zeta(z;t,f) = p_\zeta(z) = \frac{2z}{\sigma_h^2}\exp\left\{-\frac{z^2}{\sigma_h^2}\right\}, \quad z \geq 0. \tag{34}$$
This equation holds even if the gains have dissimilar variances, or if the number of multipath components is as small as $\mathcal{L} = 1$. This latter scenario ($\mathcal{L} = 1$) is clearly meaningful only

from a purely mathematical standpoint, because in practice, the Gaussianity of the channel requires the combination of several multipath components, meaning that $\mathcal{L} \gg 1$. While not shown in this paper, one can verify by proceeding as in [23], [24] that the envelope $\zeta(t,f)$ and the phase $\psi(t,f)$ are mutually statistically independent random processes [25].

C. Four-Dimensional Time-Frequency Correlation Function

The channel 4D TF-CF is defined as [26]

$$\mathcal{R}_H(t,f;\Delta t,\Delta f) \triangleq \mathcal{E}\{H^*(t-\Delta t;f)H(t;f+\Delta f)\}. \quad (35)$$

By a direct evaluation of (35), it can be shown that $\mathcal{R}_H(t,f;\Delta t,\Delta f)$ is given as in (36a) at the bottom of this page if the local IOs are randomly distributed around the receiver, where ϕ^T is given as in (29), f_D^{PW} is the Doppler frequency shift defined in (23) with the index ℓ removed, and

$$\Upsilon(t,\Delta t) \;=\; \sigma_h^2\,\Omega_{T_0}(t)\,\Omega_{T_0}(t-\Delta t). \quad (37)$$

On the other hand, we obtain (36b) if the IOs are distributed around the transmitter, where ϕ^R is the AOA defined in (30). Note that the statistical expectations in (36) are evaluated with respect to time-invariant PDFs. This is opposite to the expressions obtained by following the SWP framework, which depend on time-varying PDFs (e.g., see [9]). The results presented in (36) are therefore more mathematically tractable; although they are valid only for the small-scale statistical characterization of M2M channels. The TF-CFs in (36) incorporates the delays drifting effect through the term $\frac{1}{\mathcal{C}}[\mathcal{G}_T(\cdot)+\mathcal{G}_R(\cdot)]-tf_D^{PW}/f_c$ in the integrals' exponents. The results obtained so far by the PWP framework do not take this effect into account (see, e.g., [10]–[12]).

D. Stationarity Analysis

1) Wide-Sense Stationarity: To analyze the stationarity properties of the proposed channel model, let us first recall that a random process is called weak stationary, or WSS, if its statistical properties of the first and second order are invariant to a shift of the origin [27, Ch. 9]. For the proposed channel model, which is characterized by a 2D random process $H(t;f)$, the fulfillment of the WSS condition would imply that its mean value is constant, whereas its 4D TF-CF depends only on the 2D lag variable $(\Delta t,\Delta f)$, i.e.,

$$\mathcal{E}\{H(t;f)\} \;=\; m_H \quad (38)$$

$$\mathcal{R}_H(t_1,f_1;\Delta t,\Delta f) \;=\; \mathcal{R}_H(t_2,f_2;\Delta t;\Delta f) \quad (39)$$

for $m_H,\Delta t,\Delta f \in \mathbb{R}$, and any pair of observation points (t_1,f_1) and (t_2,f_2) in the domain of $\mathcal{R}_H(t,f;\Delta t,\Delta f)$. We note that $\mathcal{R}_H(t,f;\Delta t,\Delta f)$ is a TF-invariant function under the condition in (39). In addition, the fulfillment of (38) and (39) implies that $H(t;f)$ is simultaneously WSS in the time and the frequency domains. In the context of channel modeling, a random process that is WSS in both domains (time and frequency) is also called a WSSUS process [20]. One should keep in mind, however, that a 2D random process that does not meet the WSSUS conditions could still be a WSS process in one dimension, either in time or in frequency.

From the results presented in (36), we can conclude that the proposed channel model is a non-WSSUS process, because its 4D TF-CF is a TF-dependent function (note that the integrals at the right-hand side of (36) depend on time t and frequency f). This is a noteworthy feature, since our modeling framework does not consider shadowing, path-loss, time-varying angular statistics, or the appearance and disappearance of IOs, which are well-known causes of nonstationarities. The nonstationary characteristics of our channel model stem from the time-varying nature of the propagation delays.

Even though the proposed channel model does not fulfill the WSSUS conditions, meaning that the requirements for wide-sense stationarity cannot be met simultaneously in both the time and frequency domains, we can conclude from (36) that $H(t;f)$ is a WSS random process in the time domain if we neglect the channel's frequency selectivity, i.e., if $\Delta f = 0$. Thereby, $\mathcal{R}_H(t,f;\Delta t,\Delta f)$ becomes a time-invariant (although frequency-dependent) function, that is, $\mathcal{R}_H(t_1,f;\Delta t,\Delta f)=\mathcal{R}_H(t_2,f;\Delta t;\Delta f)$ for all $f,t_1,t_2\in\mathbb{R}$ if $\Delta f=0$. This indicates that an M2M Rayleigh fading channel can be modeled by a time-domain WSS random process for fixed values of f, i.e., for continuous-wave transmissions. Our proposed model is thus compatible with other relevant WSS narrowband Rayleigh fading channel models that have widely been in use in the past as reference models for system design, such as the model proposed by Clarke in [18]. Analogously, $H(t;f)$ becomes a frequency-domain WSS random process if we neglect the channel's time selectivity. Under this condition, $\mathcal{R}_H(t,f;\Delta t,\Delta f)$ proves to be a frequency-invariant (time-dependent) function, i.e., $\mathcal{R}_H(t,f_1;\Delta t,\Delta f)=\mathcal{R}_H(t,f_2;\Delta t;\Delta f)$, $\forall t\in[0,T_0]$ and $f_1,f_2\in\mathbb{R}$ if $\Delta t=0$.

2) Quasi-Wide-Sense Stationarity: The two particular cases discussed above are of theoretical relevance, as they allow identifying scenarios where the WSS condition is fully met, even if only in one dimension. However, such scenarios have limited practical significance. To obtain a more meaningful notion of the stationarity properties of the proposed channel model, we should turn our attention to the concept of quasi-wide-sense stationarity [28]. In this regard, we recall that

$$\mathcal{R}_H(t,f;\Delta t,\Delta f) \;=\; \Upsilon(t,\Delta t)\int_{-\pi}^{\pi} p_\phi^R(\phi)\exp\left\{-j2\pi\left[\Delta t f_D^{PW}\frac{f_c-f}{f_c}+\Delta f\left(\frac{\mathcal{G}_T(\phi^T)+\mathcal{G}_R(\phi)}{\mathcal{C}}-t\frac{f_D^{PW}}{f_c}\right)\right]\right\}\mathrm{d}\phi \quad (36a)$$

$$\mathcal{R}_H(t,f;\Delta t,\Delta f) \;=\; \Upsilon(t,\Delta t)\int_{-\pi}^{\pi} p_\phi^T(\phi)\exp\left\{-j2\pi\left[\Delta t f_D^{PW}\frac{f_c-f}{f_c}+\Delta f\left(\frac{\mathcal{G}_T(\phi)+\mathcal{G}_R(\phi^R)}{\mathcal{C}}-t\frac{f_D^{PW}}{f_c}\right)\right]\right\}\mathrm{d}\phi \quad (36b)$$

a 2D random process is deemed quasi-WSS if in spite of having time- and frequency-varying first- or/and second-order statistics, the variations of such statistics are within a given margin that allows to treat them as (quasi) invariant over finite intervals (stationarity intervals [29]) or regions (stationarity regions [28]). Hence, for a 2D quasi-WSS random process $H(t;f)$, (38) and (39) hold only as approximate relations over finite observation regions in the TF-plane.

While a thorough analysis of quasi-wide-sense stationarity is beyond the scope of this paper, some general observations can be made in that regard from (36). For example, we can observe from (36) that the frequency variations of $\mathcal{R}_H(t,f;\Delta t,\Delta f)$ are caused by the term $\Delta t f_D^{PW}(f_c-f)/f_c$. In practice, the values of f are restricted to $|f| \leq B/2$, where B is the signal's bandwidth. Given that B is typically much smaller than the carrier frequency f_c, we can use the approximation $(f_c-f)/f_c \approx 1$, which results in $\Delta t f_D^{PW}(f_c-f)/f_c \approx \Delta t f_D^{PW}$. Hence, in spite of the fact that the channel transfer function $H(t;f)$ is strictly speaking a non-WSS process in the frequency domain, we can expect its nonstationary characteristics to be fairly weak over the information signal's bandwidth. This means that the channel can be modeled by a quasi-WSS random process in the frequency domain if we consider a frequency observation interval of a length similar to the signal's bandwidth. The same observation was made empirically in [16] on the grounds of measured data. We highlight, nonetheless, that the channel's nonstationary characteristics in the frequency domain could be exacerbated significantly due to factors not considered in this paper, e.g., moving scatterers [30] or accelerated and nonlinear trajectories of the mobile stations [31].

On the other hand, we can observe from (36) that the temporal variations of $\mathcal{R}_H(t,f;\Delta t,\Delta f)$ are caused by the term $t f_D^{PW}\Delta f/f_c$, which is influenced by the degree of mobility (through the combined Doppler frequency shift f_D^{PW}), the signal's bandwidth (through the frequency lag Δf), and the carrier frequency f_c. Hence, the channel can be modeled by a quasi-WSS random process in the time domain over the region associated with $\Upsilon(t,\Delta t)\,T_0^2/\sigma_h^2$ if the user moves at a very low speed ($f_D^{PW} \approx 0$), or if the signal's bandwidth B is much smaller than f_c, such that $f_D^{PW}\Delta f/f_c \approx 0$, for $|\Delta f| \leq B$ (nearly continuous-wave transmissions).

Summarizing, we can say that even though the proposed channel model is a non-WSSUS random process, it fulfills the WSS condition in one dimension (either time or frequency) if its selectivity is negligible in the other dimension (frequency or time). This means, for example, that a small-scale frequency-nonselective line-of-sight (LOS) channel could be deemed WSS in the time domain even if its propagation delay varies over time, as intuition may suggest. The results presented in (36) also show that our channel model exhibits quasi-WSS characteristics, indicating the existence of transition regions (quasi-WSS regions) between non-WSS and WSS regions. Further research is necessary, however, to find a suitable method for determining the area of such quasi-WSS regions for a given level of tolerance in the variations of the channel's statistics. The results obtained in that regard can be used, for example, as a benchmark for analyzing and comparing the performance of existing techniques for the estimation of quasi-stationary intervals/regions of real-world M2M fading channels, e.g., those surveyed in [28] and [29].

E. Local Scattering Function, and Time-Frequency Dependent Delay and Doppler Profiles

Regarding the spectral properties of $H(t;f)$, the 2D Fourier transform of the TF-CF $\mathcal{R}_H(t,f,;\Delta t,\Delta f)$ with respect to Δt and Δf defines the TF-dependent LSF [26]

$$\mathcal{S}_H(t,f;v,\tau) \triangleq \int_{-\infty}^{\infty}\int_{-\infty}^{\infty} \mathcal{R}_H(t,f;\Delta t,\Delta f) \times \exp\{j2\pi[\tau\Delta f - v\Delta t]\}\,\mathrm{d}\Delta t\,\mathrm{d}\Delta f. \quad (40)$$

The TF-dependent LSF $\mathcal{S}_H(t,f;v,\tau)$ is a complete second-order statistic of nonstationary channels. It provides information about the channel's dispersion in the delay and Doppler frequency domains, and its definition is consistent with that of the scattering function of WSSUS channels [20, Eq. (14.1-22)]. However, in contrast to the power spectral density (PSD) of a stationary process, $\mathcal{S}_H(t,f;v,\tau)$ is not everywhere real valued or positive [26]. This shortcoming prevents from giving a clear physical interpretation of the TF-dependent LSF, and a large amount of research has been devoted to find alternative definitions of TF distribution functions (e.g., see [32] and [33]). Most notably is the generalized LSF (GLSF) $\mathcal{S}_H^G(t,f;v,\tau) \triangleq \mathcal{S}_H(t,f;v,\tau) \circledast_4 \mathcal{K}(t,f;v,\tau)$, where the operator $\circledast_x$ denotes the x-dimensional convolution, and $\mathcal{K}(t,f;v,\tau)$ is a kernel function [26]. The GLSF $\mathcal{S}_H^G(t,f;v,\tau)$ is always real-valued and positive. It is similar in that respect to the PSD of a stationary process [26]. Nonetheless, the computation of a proper kernel function for the evaluation of $\mathcal{S}_H^G(t,f;v,\tau)$ is out of the paper's scope. For this reason, we will restrict our attention to the LSF defined by (40) and to the particular cases stemming from it.

Assuming that the IOs are randomly located around the receiver, we find by substituting (36a) into (40) that

$$\begin{aligned}\mathcal{S}_H(t,f;v,\tau) &= \sigma_h^2\,T_0\,\Omega_{T_0}(t)\int_{-\pi}^{\pi} p_\phi^R(\phi) \\ &\quad\times\exp\left\{-j2\pi\left(v+f_D^{PW}\frac{f_c-f}{f_c}\right)\left(t-\frac{T_0}{2}\right)\right\} \\ &\quad\times\mathrm{sinc}\left(\pi T_0\left[v+f_D^{PW}\frac{f_c-f}{f_c}\right]\right) \\ &\quad\times\delta\left(\tau-\frac{\mathcal{G}_T(\phi_T)+\mathcal{G}_R(\phi)}{\mathcal{C}}+t\frac{f_D^{PW}}{f_c}\right)\mathrm{d}\phi. \quad (41)\end{aligned}$$

The channel's dispersion in the delay domain is characterized by the TF-dependent delay profile [26]

$$\mathcal{P}_H(t,f;\tau) \triangleq \int_{-\infty}^{\infty} S_H(t,f;v,\tau)\,\mathrm{d}v \quad (42)$$

$$= \int_{-\infty}^{\infty} R_H(t,f;0,\Delta f) \times\exp\{j2\pi\tau\Delta f\}\,\mathrm{d}\Delta f. \quad (43)$$

In turn, the dispersion in the Doppler frequency domain is characterized by the TF-dependent Doppler profile [26]

$$\mathcal{D}_H(t,f;v) \triangleq \int_{-\infty}^{\infty} S_H(t,f;v,\tau)\,\mathrm{d}\tau \tag{44}$$

$$= \int_{-\infty}^{\infty} R_H(t,f;\Delta t,0) \times \exp\{-j2\pi v\Delta t\}\,\mathrm{d}\Delta t. \tag{45}$$

For the LSF in (41), we have:

$$\mathcal{P}_H(t,f;\tau) = \sigma_h^2\,\Omega_{T_0}(t)\int_{-\pi}^{\pi} p_\phi^R(\phi) \times\delta\left(\tau - \frac{\mathcal{G}_T(\phi_T)+\mathcal{G}_R(\phi)}{\mathcal{C}} + t\frac{f_D^{PW}}{f_c}\right)\mathrm{d}\phi \tag{46}$$

$$\mathcal{D}_H(t,f;v) = \sigma_h^2\,T_0\,\Omega_{T_0}(t)\int_{-\pi}^{\pi} p_\phi^R(\phi) \times\exp\left\{-j2\pi\left(v + f_D^{PW}\frac{f_c-f}{f_c}\right)\left(t-\frac{T_0}{2}\right)\right\} \times\mathrm{sinc}\left(\pi T_0\left[v + f_D^{PW}\frac{f_c-f}{f_c}\right]\right)\mathrm{d}\phi. \tag{47}$$

Equation (46) shows that the TF-dependent delay profile $\mathcal{P}_H(t,f;\tau)$ of the proposed channel model does not depend on the frequency f variable. This is due to the fact that we have not considered group delay dispersion for the definition of the CIR $h(t;\tau)$ given by (1), as pointed out at the end of Section II.[2] On the other hand, the delay profile $\mathcal{P}_H(t,f;\tau)$ is a time-varying function, as was to be expected, since the propagation delays of the received waves change over time due to the drifting effect. To simplify our notation, we will hereafter denote the delay profile by $\mathcal{P}_H(t;\tau)$. In turn, the result in (47) shows that the TF-dependent Doppler profile $\mathcal{D}_H(t,f;v)$ varies in both the time and the frequency domains. The frequency dependence of $\mathcal{D}_H(t,f;v)$ indicates that the "frequency modulation" effects caused by the channel's dispersion in the Doppler frequency domain are different for each spectral component of the transmitted signal. In practice, however, such differences can be expected to be small, since $(f_c-f)/f_c \approx 1$ within the signal's bandwidth.

VI. The Geometrical One-Ring Scattering Model

In this section, we present a novel approximate closed-form solution of (36) by considering the particular case of the propagation scenario shown in Fig. 4, where the IOs are located on a ring of radius d centered on $\mathcal{O}'$. In addition, we present some numerical results that illustrate the remarks we made in the previous section about $\mathcal{R}_H(t,f;\Delta t,\Delta f)$, $\mathcal{P}_H(t;\tau)$, and $\mathcal{D}_H(t,f;v)$. For that purpose, we will assume that the AOAs ϕ_ℓ^R follow the von Mises distribution [34] with mean $\mu \in [-\pi,\pi)$ and concentration parameter κ, $0 \le \kappa < \infty$,

[2]The effects of group delay distortion should be taken into account, nonetheless, for wireless communication system operating with very large bandwidths, such as the emerging mm-Band wireless communication systems.

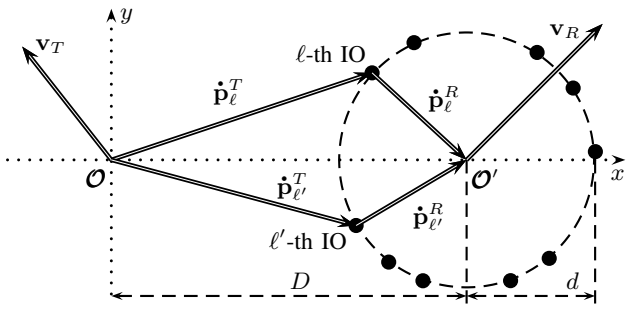

Fig. 4. Illustration of the geometrical one-ring scattering model.

in such a way that $p_\phi^R(\phi) = \exp\{\kappa\cos(\phi-\mu)\}/(2\pi I_0(\kappa))$, $\phi \in [-\pi,\pi)$, where $I_0(\cdot)$ is the modified Bessel function of the first kind and zero order. The use of the von Mises PDF to model the AOA statistics of mobile fading channels was originally proposed in [35]. In that paper, the authors provide evidence of the suitability of such a PDF to match measured data. This model has widely been employed for the statistical analysis of F2M and M2M fading channels [10]–[12], [14].

A. Four-Dimensional Time-Frequency Correlation Function for the Geometrical One-Ring Model

For the geometrical one-ring scattering model shown in Fig. 4, and assuming that the condition $d \ll D$ is fulfilled, meaning that the mobile terminals are far enough from each other, one can verify that (see Appendix B)

$$\mathcal{R}_H(t,f;\Delta t,\Delta f) \approx \Upsilon(t,\Delta t) \times\frac{\exp\{-j2\pi\mathcal{A}(t,f;\Delta t,\Delta f)\}}{I_0(\kappa)} \times I_0\Bigg(\Big\{\big[\kappa\cos(\mu) - j2\pi\mathcal{B}_c(t,f;\Delta t,\Delta f)\big]^2 + \big[\kappa\sin(\mu) - j2\pi\mathcal{B}_s(t,f;\Delta t,\Delta f)\big]^2\Big\}^{1/2}\Bigg) \tag{48}$$

where:

$$\mathcal{A}(t,f;\Delta t,\Delta f) = \mathcal{Z}(t,f;\Delta t,\Delta f)f_{\max}^T\cos(\gamma_T) + \Delta f\left(\frac{D+d}{\mathcal{C}}\right) \tag{49a}$$

$$\mathcal{B}_c(t,f;\Delta t,\Delta f) = \mathcal{Z}(t,f;\Delta t,\Delta f)f_{\max}^R\cos(\gamma_R) - \Delta f\frac{d}{\mathcal{C}} \tag{49b}$$

$$\mathcal{B}_s(t,f;\Delta t,\Delta f) = \mathcal{Z}(t,f;\Delta t,\Delta f)\Big[f_{\max}^T\frac{d}{D}\sin(\gamma_T) + f_{\max}^R\sin(\gamma_R)\Big] \tag{49c}$$

$$\mathcal{Z}(t,f;\Delta t,\Delta f) = \Delta t\left(\frac{f_c-f}{f_c}\right) - \Delta f\frac{t}{f_c}. \tag{49d}$$

The 4D TF-CF in (48) and (49) includes as special cases other relevant correlation models for multipath fading channels. For example, we obtain the correlation model proposed by Clarke in [18] for isotropic scattering F2M channels if we take $\kappa = 0$, $f_{\max}^T = 0$, $\gamma_T =$

0°, and $\Delta f \approx 0$ (narrowband communications) in (48) and (49). Under these conditions, and taking into account that $(f_c - f)/f_c \approx 1$, we have $\mathcal{R}_H(t,f;\Delta t,\Delta f) \approx \Upsilon(t,\Delta t)\, J_0(2\pi f^R_{\max}\Delta t)$. Under the same conditions, but taking $\kappa \neq 0$, we find that $\mathcal{R}_H(t,f;\Delta t,\Delta f) \approx \Upsilon(t,\Delta t)\, I_0(\sqrt{\kappa^2 - (2\pi f^R_{\max}\Delta t)^2 - j4\pi\kappa\cos(\mu) f^R_{\max}\Delta t})/I_0(\kappa)$. This latter result can be identified as the correlation model proposed by Abdi, Barger, and Kaveh in [13] for non-isotropic scattering F2M channels. Thus, the 4D TF-CF presented in this section can be seen as a generalization of such correlation models with respect to nonstationary TF-dispersive M2M channels.

B. Time-Frequency Dependent Delay and Doppler Profiles for the Geometrical One-Ring Model

The Fourier transform of the modified Bessel function in (48) cannot be written in a closed form for the mapping $(\Delta t,\Delta f) \longmapsto (v,\tau)$. For this reason, the LSF associated to the 4D TF-CF presented in (48) has to be evaluated numerically. The numerical analysis simplifies significantly if one considers the TF-dependent delay and Doppler profiles $\mathcal{P}_H(t;\tau)$ and $\mathcal{D}_H(t,f;v)$ instead of the LSF. Substituting (48) into (43) and (45), we obtain:

$$\begin{aligned}\mathcal{P}_H(t;\tau) \;\approx\; & \frac{\sigma_h^2\,\Omega_{T_0}(t)}{I_0(\kappa)} \\ & \times \int_{-\infty}^{\infty} \exp\left\{j2\pi\left[\Delta f\tau - \mathcal{A}(t,f;0,1)\right]\right\} \\ & \times I_0\Bigg(\Big\{\big[\kappa\cos(\mu) - j2\pi\mathcal{B}_c(t,f;0,\Delta f)\big]^2 \\ & + \big[\kappa\sin(\mu) - j2\pi\mathcal{B}_s(t,f;0,\Delta f)\big]^2\Big\}^{1/2)}\Bigg)\,\mathrm{d}\Delta f \quad (50)\end{aligned}$$

$$\begin{aligned}\mathcal{D}_H(t,f;v) \;\approx\; & \frac{\sigma_h^2\,\Omega_{T_0}(t)}{I_0(\kappa)} \\ & \times \int_{t-T_0}^{t} \exp\left\{-j2\pi\left[\Delta t v + \mathcal{A}(t,f;1,0)\right]\right\} \\ & \times I_0\Bigg(\Big\{\big[\kappa\cos(\mu) - j2\pi\mathcal{B}_c(t,f;\Delta t,0)\big]^2 \\ & + \big[\kappa\sin(\mu) - j2\pi\mathcal{B}_s(t,f;\Delta t,0)\big]^2\Big\}^{1/2}\Bigg)\,\mathrm{d}\Delta t. \quad (51)\end{aligned}$$

C. Numerical Examples

To illustrate the observations we made in Section V about the correlation and spectral properties of the proposed channel model, we will consider the modeling of a TF dispersive M2M channel for IEEE 802.11p-based DSRC systems [4]. For the modeling of such a channel, we have considered the parameters summarized in Table I. The length of the observation window $T_0 = 6.4$ ms corresponds to the length of a data frame comprising 600 OFDM symbols. In turn, the 200 Hz value of the maximum Doppler frequencies corresponds to a speed of 37 km/h. The domain of $\mathcal{R}_H(t,f;\Delta t,\Delta f)$ spans the region defined by $t \in [0,T_0]$, $\Delta t \in [t-T_0,t]$, $f \in (-\infty,\infty)$, and $\Delta f \in (-\infty,\infty)$. However, for practical purposes, the relevant region is bounded by the system's bandwidth B, in such a way that $|f| \leq B/2$, and $|\Delta f| \leq B$. Unless otherwise stated, we will work with such a reduced domain.

TABLE I
SIMULATION PARAMETERS

Description	Value
Average power of the channel (σ_h^2)	$\sigma_h^2 = 1$
Carrier frequency (f_c)	$f_c = 5.9$ GHz
System's bandwidth (B)	$B = 10$ MHz
Length of the observation window $\Omega_{T_0}(t)$ (T_0)	$T_0 = 6.4$ ms
Maximum Doppler frequency due to the transmitter's speed ($f^T_{\max}$)	$f^T_{\max} = 200$ Hz
Maximum Doppler frequency due to the receiver's speed ($f^R_{\max}$)	$f^R_{\max} = 200$ Hz
Azimuth direction of motion of the transmitter (γ_T)	$\gamma_T = 45^\circ$
Azimuth direction of motion of the receiver (γ_R)	$\gamma_R = 225^\circ$
Initial distance between the transmitter and the receiver (D)	$D = 500$ m
Radius of the ring of scatterers (d)	$d = 30$ m

1) 4D Time-Frequency Correlation Function: Figure 5 shows the absolute value of $\mathcal{R}_H(t,f;\Delta t,\Delta f)$ evaluated at four different observation points in the TF plane. The 2D correlation functions (CFs) shown in this figure are similar to the spaced-frequency spaced-time (SF-ST) CF of WSSUS fading channels [20] in the sense that they also characterize the channel correlation around a reference observation point (t,f). However, in contrast to the SF-ST CF, which is invariant in both the time t and the frequency f variables, the shape of the CFs shown in Fig. 5 varies from one observation point to another; this is a distinctive characteristic of nonstationary processes. The graphs presented in Fig. 5 also show that the channel 4D TF-CF varies more rapidly in time than in frequency. These results suggest that the nonstationarities of the proposed channel model are stronger in the time domain than in the frequency domain. In fact, by comparing Figs. 5(a) and 5(c) (or Figs. 5(b) and 5(d)), it might seem that $|\mathcal{R}_H(t,f;\Delta t,\Delta f)|$ is a frequency invariant function, which in turn could be interpreted as an indication of the channel being a frequency-domain WSS random process. Nevertheless, this is not a correct appreciation, since $\mathcal{R}_H(t,f;\Delta t,\Delta f)$ does vary over frequency, but at a rate that is much larger than the system's bandwidth. This can readily be seen if one compares Figs. 5(c) and 5(d) with Figs. 6(a) and 6(b), respectively. Note that in Fig. 6, the reference observation frequency is 1000 times larger than that in Figs. 5(c) and 5(d).

The nonstationary characteristics of $H(t;f)$ in the frequency-domain are further evinced by the lack of symmetry of $|\mathcal{R}_H(t,f;\Delta t,\Delta f)|$ around $\Delta f = 0$; recall that a WSS random process is Hermitian symmetric around the origin [36,

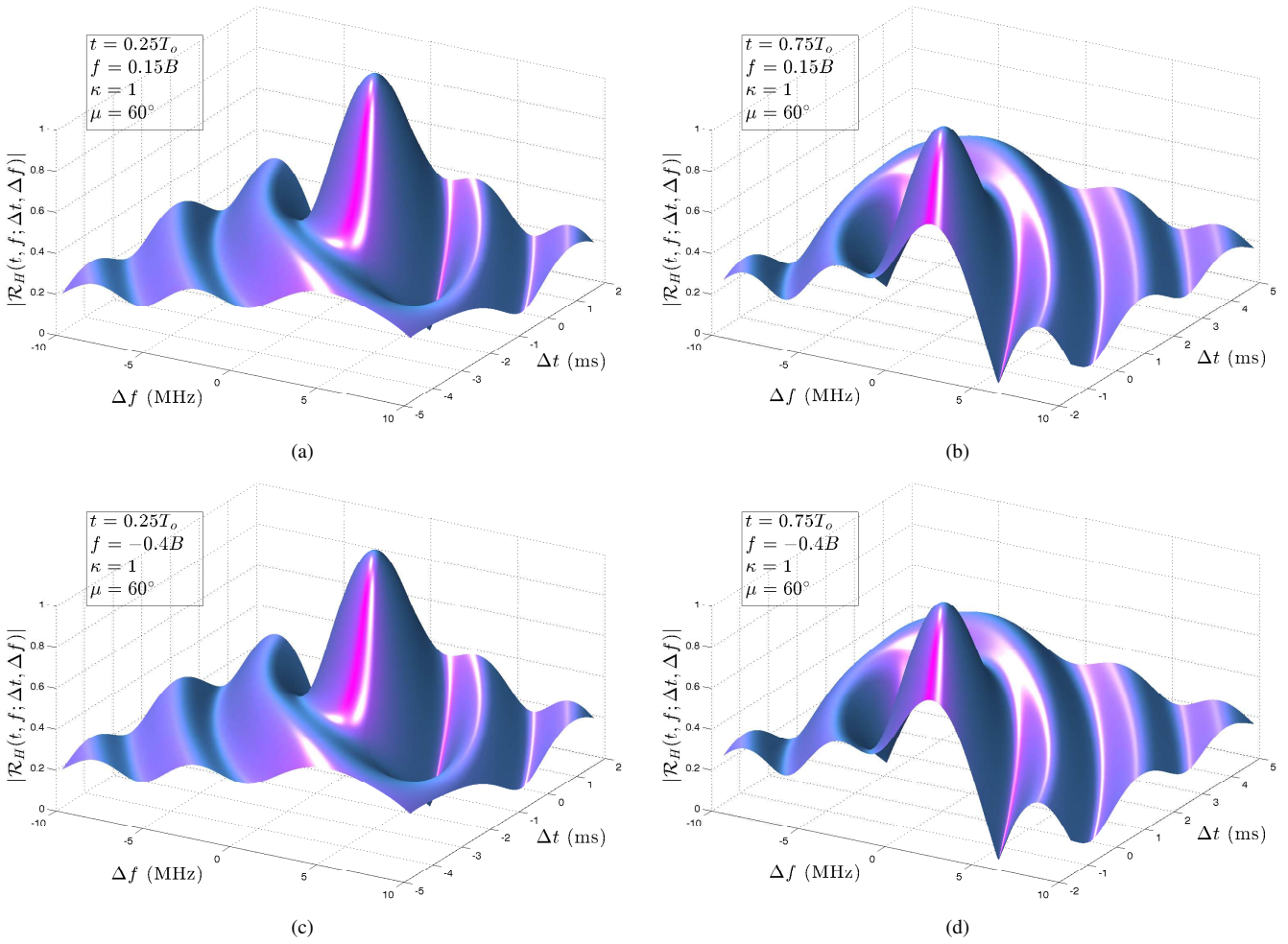

Fig. 5. Absolute value of the 4D TF-CF $\mathcal{R}_H(t, f; \Delta t, \Delta f)$ at four different observation points (t, f) with $t \in \{0.25\,T_0, 0.75\,T_0\}$ and $f \in \{0.15B, -0.4B\}$.

Theorem 10.12]. To make this fact apparent, we plot in Fig. 7 the absolute value of the 4D TF-CF for two observation points in the $(t, \Delta t)$-plane: one with $t = 0.25T_0$ and $\Delta t = -0.5T_0$, and the other with $t = 0.25T_0$ and $\Delta t = 0$. Note that the resulting 2D CFs are analogous to the frequency CF (FCF) of WSSUS channels, as they also describe the channel's frequency-correlation properties for fixed values of t and Δt.

The graph of $|\mathcal{R}_H(t, f; \Delta t, \Delta f)|$ shown in Fig. 7(a) is clearly asymmetric. This indicates that for the chosen observation point $(t = 0.25T_0, \Delta t = -0.5T_0)$, the channel is a frequency-domain non-WSS process. A different scenario is presented in Fig. 7(b) with $\Delta t = 0$, where $|\mathcal{R}_H(t, f; \Delta t, \Delta f)|$ is symmetric around $\Delta f = 0$, and reaches a maximum also at $\Delta f = 0$, meaning that $h(t; \tau)$ is a frequency-domain WSS process [36, Theorem 10.12]). This is not surprising, as we pointed out in Section V-C that the channel is a WSS process in the frequency domain if $\Delta t = 0$, i.e., if the length of the observation time window is infinitely small (note that $\Delta t = 0$ for the example presented in Fig. 7(b)). In fact, the shape of $|\mathcal{R}_H(t, f; \Delta t, \Delta f)|$ gradually becomes symmetric about the Δf variable as Δt approaches to zero. This means that for "sufficiently small" values of Δt, $|\mathcal{R}_H(t, f; \Delta t, \Delta f)|$ can be presumed to be symmetric about the Δf-axis, and the proposed channel model can in turn be considered as quasi-WSS in the frequency domain.

Similarly, we show in Fig. 8 the absolute value of the 4D TF-CF for two observation points in the $(f, \Delta f)$ plane: one with $f = 0.15B$ and $\Delta f = -0.6B$, and the other with $f = 0.15B$ and $\Delta f = 0$. The CFs presented in this figure are analogous to the time CF (TCF) of WSSUS channels. Nevertheless, in addition to being frequency dependent, the domain of the CFs in Fig. 8 is constrained to $t \in [0, T_0]$ and $\Delta t \in [t - T_0, t]$. The symmetries of $\mathcal{R}_H(t, f; \Delta t, \Delta f)$ around $\Delta t = 0$ are not easy to assess from Fig. 8 because of such a truncated domain. However, taking the projection of $\mathcal{R}_H(t, f; \Delta t, \Delta f)$ onto an arbitrary plane defined for a fixed t (and given that f and Δf have also been fixed), we obtain the curves shown in Fig. 9. This latter figure suggests that the channel is a time-domain WSS process within the observation time window if $\Delta f = 0$, but it is otherwise a non-WSS process. Again, we observe that $|\mathcal{R}_H(t, f; \Delta t, \Delta f)|$ becomes a symmetric function in the Δt variable as Δf approaches to zero, indicating that our channel model may be considered quasi-WSS in the time domain for small values of Δf.

2) Time-Frequency Dependent Delay Profile: Regarding the channel's dispersion in the delay domain, we present plots

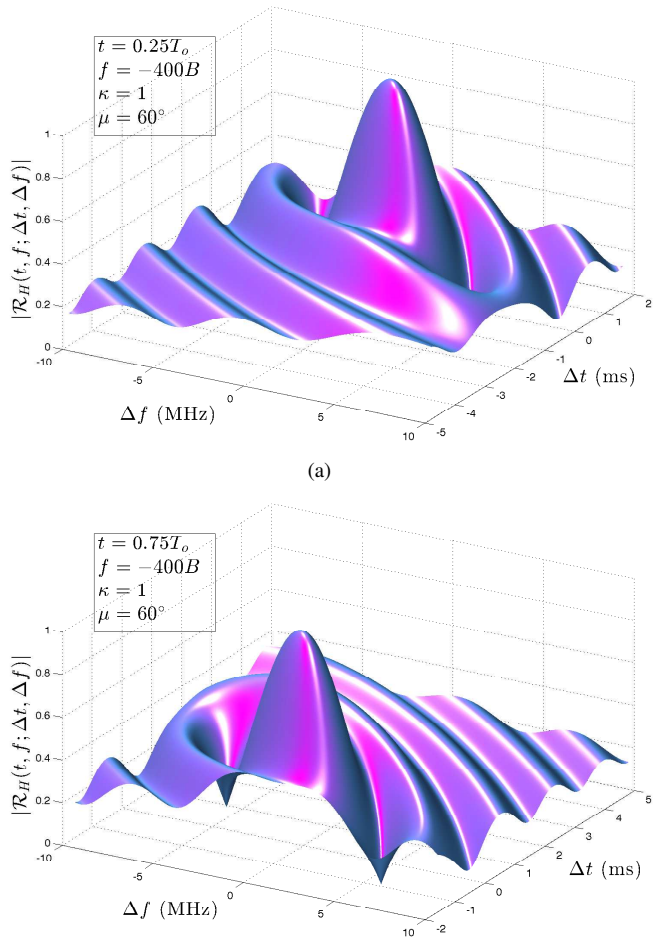

Fig. 6. Absolute value of the 4D TF-CF $\mathcal{R}_H(t, f; \Delta t, \Delta f)$ at two different observation points (t, f) with $t \in \{0.25\,T_0, 0.75\,T_0\}$ and $f = -400B$.

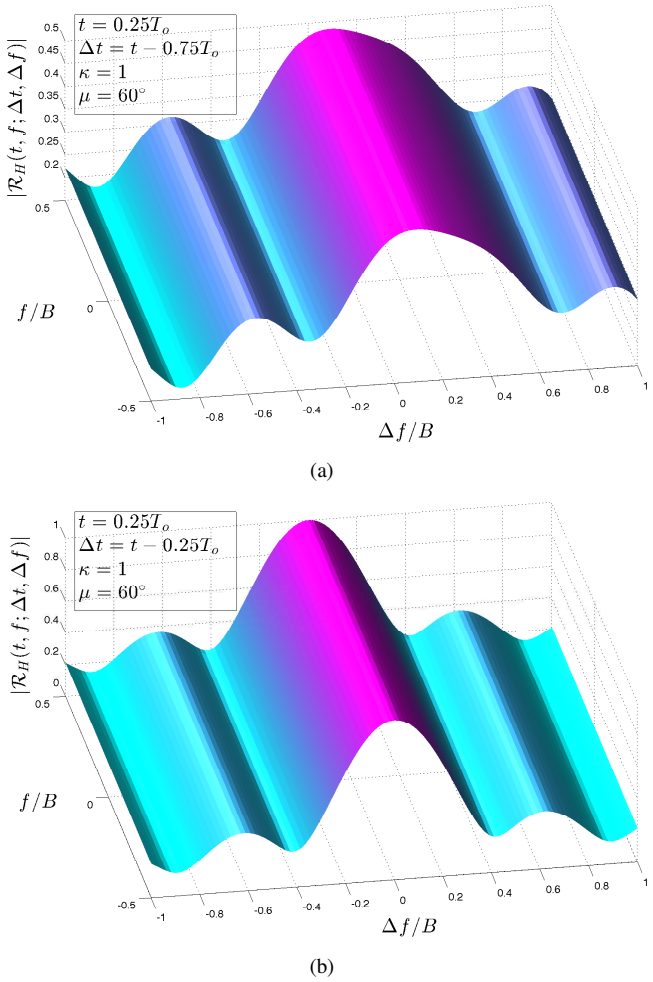

Fig. 7. Absolute value of the 4D TF-CF $\mathcal{R}_H(t, f; \Delta t, \Delta f)$ at two observation points $(t, \Delta t)$ with $t = 0.25T_0$ and $\Delta t \in \{t - 0.75T_0, t - 0.25T_0\}$.

of the normalized absolute value of the TF-dependent delay profile $\mathcal{P}_H(t; \tau)$ in Fig. 10. The graphs shown in this figure were generated by evaluating (50) for: $f = 0$ (the value of f is in fact irrelevant, because $\mathcal{P}_H(t; \tau)$ is a frequency-invariant function), $f^T_{\max} = f^R_{\max} = 500$ Hz (corresponding to a speed of 91 km/h), $(\gamma_T, \gamma_R) \in \{(45^\circ, 165^\circ), (165^\circ, 45^\circ)\}$, and $T_0 = 320$ ms (corresponding to the duration of 50 IEEE 802.11p-based data frames, each comprising 800 OFDM symbols). The values of the maximum Doppler frequencies ($f^T_{\max}$ and $f^R_{\max}$) and the length T_0 of the observation time window have been increased with respect to the examples presented in Figs. 5–9 to highlight the variability in time of $\mathcal{P}_H(t; \tau)$. This modification does not compromise the validity of the results presented in (48) and (50), since for the given values of $f^T_{\max} = 500$ Hz, $f^R_{\max} = 500$ Hz, $T_0 = 320$ ms, and $d = 30$ m, we can guarantee that the receiver is always nearby the reference point $\mathcal{O}'$ (see Fig. 2). This condition has to be fulfilled to ensure that the receiver antenna will be within the path of the plane waves that propagate from the ring of IOs towards $\mathcal{O}'$. Note that the time taken by the receiver to move from the center to the border of the ring is equal to 1.18 s, which is more than three times the chosen value of T_0.

The graphs shown in Fig. 10 provide a clear illustration of the propagation delay's temporal evolution. In the example presented in Figs. 10(a) and 10(b), the receiver and the transmitter are moving toward each other (although not directly). For this reason, the maximum excess delay shrinks as t increases. On the other hand, in the example presented in Figs. 10(c) and 10(d), the mobile stations are moving away from each other. The maximum excess delay therefore increases as t increases. Figure 10 also show that for $t = 0$, the minimum and maximum excess delays are approximately equal to 1.67 µs and 200 ns, respectively. This is consistent with the geometry of the propagation scenario, since a traveling wave takes $D/\mathcal{C} = 1.667$ µs to cover the distance $D = 500$ m between the mobile terminals at $t = 0$, and it takes an additional time of $2d/\mathcal{C} = 200.13$ ns to travel over the longest path.

3) TF Dependent Doppler Profile: Finally, we show in Fig. 11 the normalized absolute value of the TF-dependent Doppler profile $\mathcal{D}_H(t, f; v)$ for $|f| \leq B/2$, $|v| \leq 2(f^T_{\max} + f^R_{\max})$, and $t \in \{0.1\,T_0, 0.8\,T_0\}$. Again, we consider: $f^T_{\max} = f^R_{\max} = 500$ Hz, and $(\gamma_T, \gamma_R) \in \{(45^\circ, 165^\circ), (165^\circ, 45^\circ)\}$. However, for the evaluation of (51), we set $T_0 = 6.4$ ms.

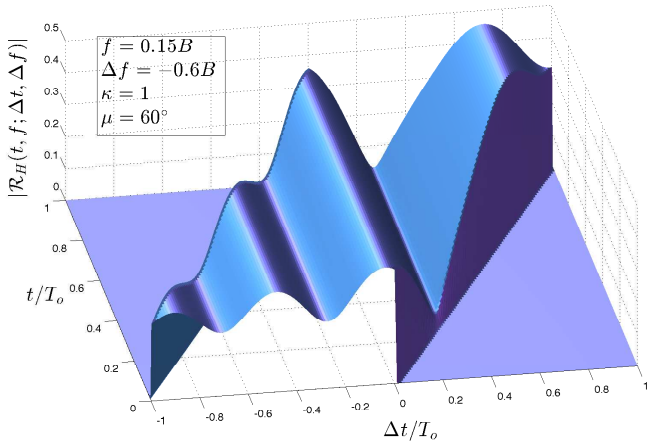

(a)

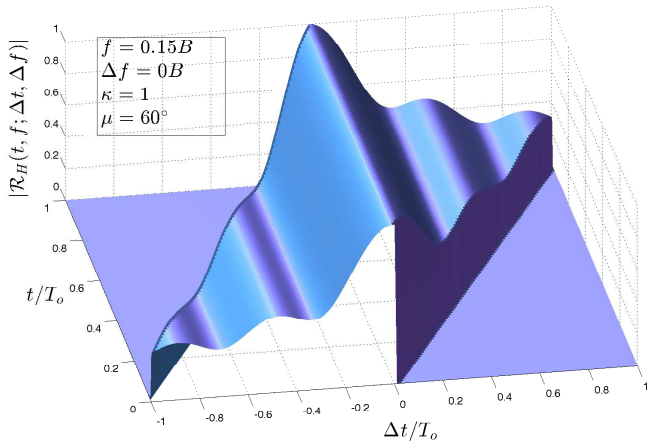

(b)

Fig. 8. Absolute value of the 4D TF-CF $\mathcal{R}_H(t, f; \Delta t, \Delta f)$ at two observation points $(f, \Delta f)$ with $f = 0.15B$ and $\Delta f \in \{-0.6B, 0\}$.

One can readily observe from the graphs presented in Fig. 11 that $\mathcal{D}_H(t, f; v)$ is a time-varying function, as mentioned in Section V-E. Nonetheless, the variability of $\mathcal{D}_H(t, f; v)$ in the frequency domain cannot be appreciated from this figure due to the short observation frequency interval. To demonstrate that $\mathcal{D}_H(t, f; v)$ is a frequency-varying function, we present in Fig. 12 the color map of the surface in Fig. 11(c) and the color map of the same surface but for a larger observation window, $|f| \leq 100B$. This figure shows that the shape of $|\mathcal{D}_H(t, f; v)|$ does change in frequency, but at a very low rate. This is consistent with the observations made at the end of Section V-E.

VII. Conclusions

In this paper, we proposed a novel GBSM for small-scale non-WSSUS M2M Rayleigh fading channels. Based on this model, we derived general analytic expressions for the first-order PDFs of the envelope and phase, the 4D TF-CF, LSF, and TF-dependent delay and Doppler profiles. In addition, by assuming that the IOs are randomly located on a ring surrounding the receiver, we derived a novel approximate closed-form expression for the channel 4D TF-CF. The analytical

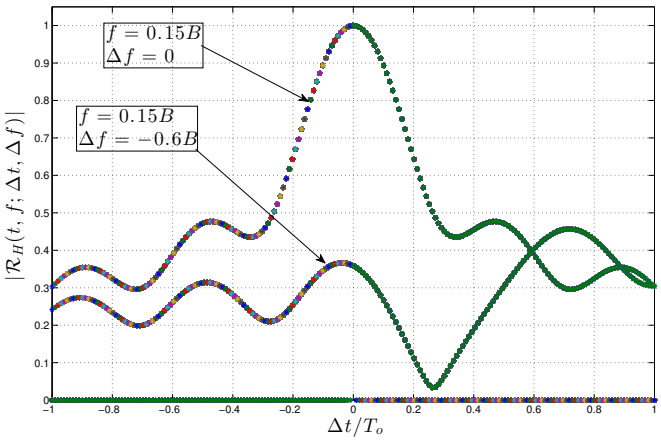

Fig. 9. Projections of the surfaces shown in Fig. 8 onto an arbitrary plane in which t is fixed.

and numerical results presented here provide new insights into the correlation and spectral properties of nonstationary M2M Rayleigh fading channels. Our results indicate that for the propagation over small local areas, the channel's nonstationarities are determined by the propagation environment (through the geometrical configuration of the propagation area) and the transmission system's frequency range. In the frequency domain, the nonstationarities are influenced by the ratio of the transmitted signal bandwidth B to the carrier frequency f_c, whereas in the time domain, they are influenced by the degree of mobility, the signal's bandwidth, and the carrier frequency. Even though the proposed channel model is a non-WSSUS random process, it approximately fulfills the WSS condition in one dimension (either time or frequency) if its selectivity is negligible in the other dimension (frequency or time). Furthermore, the obtained results suggest the existence of transition regions (quasi-WSS regions) between non-WSS and WSS characteristics.

The conclusions drawn here are in good agreement with empirical observations made independently in previous papers. However, further research is necessary to obtain a representative measurement data base that allows for a thorough validation of the proposed channel model. Future work also calls for an in-depth analysis of the quasi-WSS properties of channel models to accurately identify quasi-WSS regions in the time and/or frequency dimensions.

Appendix A
Derivation of the PDF in (34)

If the random gains g_ℓ are characterized by a Rayleigh distribution, in such a way that $p_\ell^g(z) = \frac{z}{\sigma_\ell^2} \exp\{-z^2/(2\sigma_\ell^2)\}$, where $\sigma_\ell \neq \sigma_k$ for $\ell \neq k$, then

$$\begin{aligned} p_\zeta(z; t, f) &= (2\pi)^2 z \\ &\quad \times \int_0^\infty \left[\prod_{\ell=1}^{\mathcal{L}} \int_0^\infty \frac{y_\ell}{\sigma_\ell^2} \exp\left\{ -\frac{y_\ell^2}{2\sigma_\ell^2} \right\} J_0(2\pi x y_\ell)\, \mathrm{d}\ell \right] \\ &\quad \times J_0(2\pi z x) x\, \mathrm{d}x, \quad z \geq 0. \end{aligned} \tag{52}$$

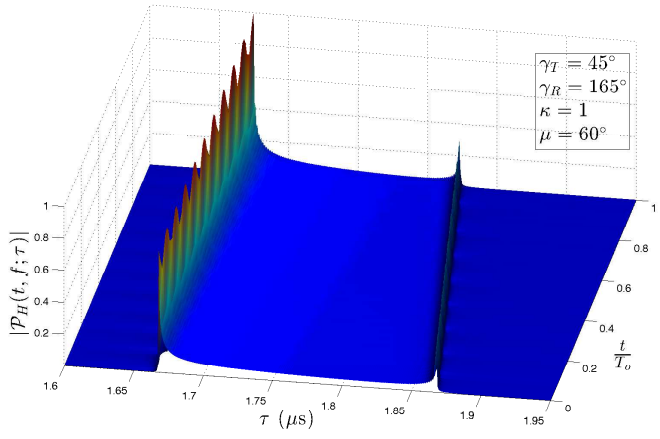

(a) 3D surface of $|\mathcal{P}_H(t;\tau)|$ for $\gamma_T = 45°$ and $\gamma_R = 165°$

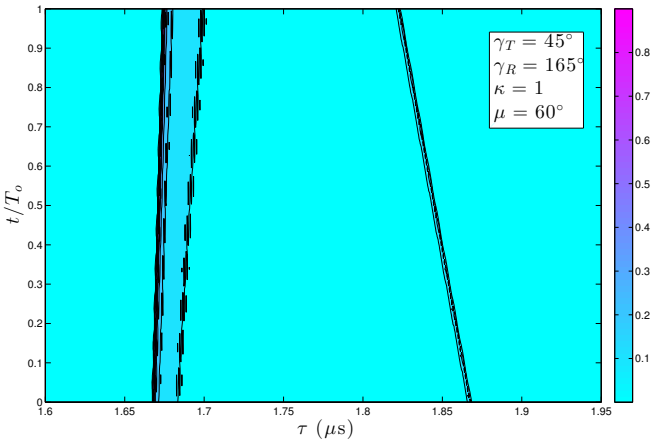

(b) Color map of $|\mathcal{P}_H(t;\tau)|$ for $\gamma_T = 45°$ and $\gamma_R = 165°$

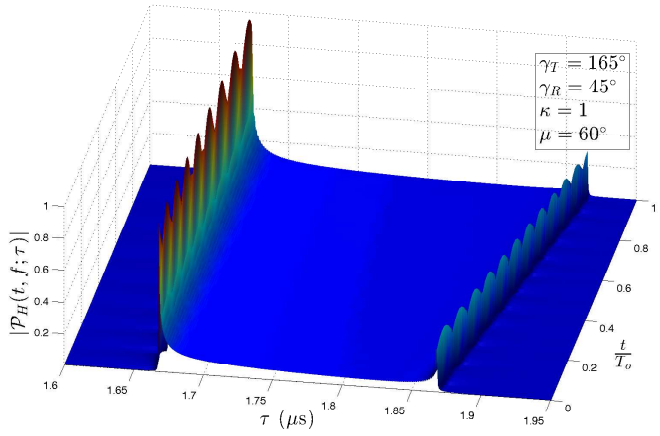

(c) 3D surface of $|\mathcal{P}_H(t;\tau)|$ for $\gamma_T = 165°$ and $\gamma_R = 45°$

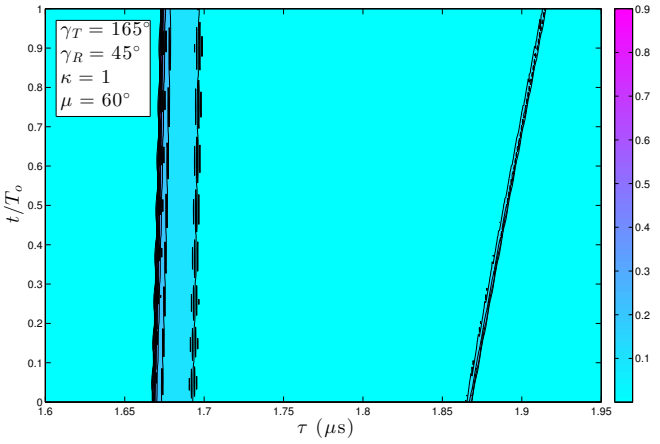

(d) Color map of $|\mathcal{P}_H(t;\tau)|$ for $\gamma_T = 165°$ and $\gamma_R = 45°$

Fig. 10. Absolute value of the TF-dependent delay profile $\mathcal{P}_H(t;\tau)$ with $f = 0$ and $f^T_{\max} = f^R_{\max} = 500$ Hz.

Using [37, Eq. (6.631-4)] to solve the innermost integral, we find

$$\begin{aligned} p_\zeta(z;t,f) &= (2\pi)^2 z \\ &\times \int_0^\infty \left[\prod_{\ell=1}^{\mathcal{L}} \exp\left\{-2\pi^2 x^2 \sigma_\ell^2\right\}\right] J_0(2\pi z x) x \,\mathrm{d}x \\ &= (2\pi)^2 z \\ &\times \int_0^\infty \left[\exp\left\{-2\pi^2 x^2 \left(\sum_{\ell=1}^{\mathcal{L}} \sigma_\ell^2\right)\right\}\right] J_0(2\pi z x) x \,\mathrm{d}x. \quad (53) \end{aligned}$$

The second moment of the ℓth Rayleigh distributed random gain g_ℓ is equal to $\mathcal{E}\{|g_\ell|^2\} = 2\sigma_\ell^2$. Hence,

$$\sum_{\ell=1}^{\mathcal{L}} \sigma_\ell^2 = \frac{1}{2}\sum_{\ell=1}^{\mathcal{L}} \mathcal{E}\{|g_\ell|^2\} = \frac{1}{2}\sigma_h^2 \quad (54)$$

where we have made use of (27). Then, substituting this result into (53), and using [37, Eq. (6.633-2)], we obtain (34).

Appendix B
Derivation of the Time-Frequency Correlation Function in (48)

For the geometrical one-ring scattering model at the receiver side, we have

$$d_\ell^T = \|\dot{\mathbf{p}}_\ell^T\| = D\sqrt{1 + \left(\frac{d}{D}\right)^2 - \frac{2d}{D}\cos(\phi_\ell^R)} \quad (55)$$

$$d_\ell^R = \|\dot{\mathbf{p}}_\ell^R\| = d \quad (56)$$

for all $\ell = 1, 2, \ldots, \mathcal{L}$. If the mobile terminals are far enough from each other, in such a way that $d \ll D$, then $d/D \ll 1$ and $(d/D)^2 \approx 0$. Hence, using the approximate relation $\sqrt{1+\chi} \approx 1 + \chi/2$, for $|\chi| \ll 1$ (cf. [37, Eq. (1.112-3)]), we can rewrite (55) as

$$d_\ell^T \approx D - d\cos(\phi_\ell^R), \quad \forall \ell = 1, 2, \ldots, \mathcal{L}. \quad (57)$$

Under the same condition, and taking into account that $\arctan(\chi) \approx \chi$, if $\chi \approx 0$ [37, Eq. (1.643-1)], we can approximate the AODs defined in (29) by

$$\phi_\ell^T \approx \frac{d}{D}\sin(\phi_\ell^R), \quad \forall \ell = 1, 2, \ldots, \mathcal{L}. \quad (58)$$

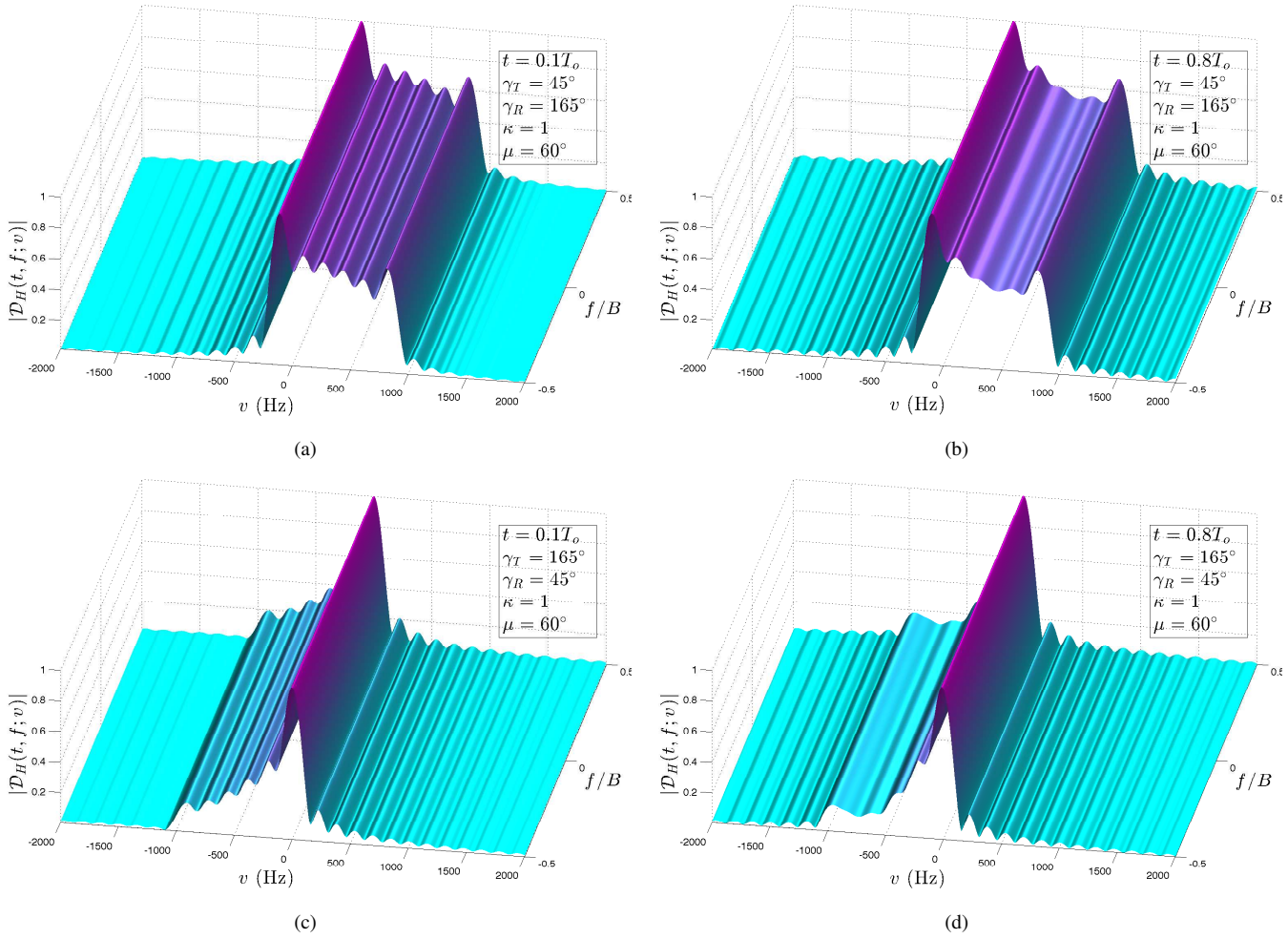

Fig. 11. Absolute value of the TF-dependent Doppler profile $\mathcal{D}_H(t, f; v)$ evaluated for $|f| \leq B/2$, $|v| \leq 2(f^T_{\max} + f^R_{\max})$, and $t \in \{0.1\,T_0, 0.8\,T_0\}$.

Based on (57) and (58), and using the small-argument approximations $\cos(\chi) \approx 1$, and $\sin(\chi) \approx \chi$ [37, Eqs. (1.411-1,3)]), we can write:

$$\frac{\mathcal{G}_T(\phi^T_\ell) + \mathcal{G}_R(\phi^R_\ell)}{\mathcal{C}} \approx \frac{D+d}{\mathcal{C}} - \frac{d\cos(\phi^R_\ell)}{\mathcal{C}} \tag{59}$$

$$\begin{aligned} f^{PW}_D \approx\ & f^T_{\max}\cos(\gamma_T) \\ & + \cos(\phi^R_\ell) f^R_{\max}\cos(\gamma_R) \\ & + \sin(\phi^R_\ell)\Big[f^T_{\max}\frac{d}{D}\sin(\gamma_T) \\ & + f^R_{\max}\sin(\gamma_R)\Big] \end{aligned} \tag{60}$$

if $d \ll D$. Substituting (59) and (60) into (36a), we find that

$$\begin{aligned} \mathcal{R}_H(t, f; \Delta t, \Delta f) \approx\ & \Upsilon(t, \Delta t)\exp\{-j2\pi\mathcal{A}(t, f; \Delta t, \Delta t)\} \\ & \times \int_{-\pi}^{\pi} \exp\Big\{ - j2\pi\big[\mathcal{B}_c(t, f; \Delta t, \Delta t)\cos(\phi) \\ & + \mathcal{B}_s(t, f; \Delta t, \Delta t)\sin(\phi)\big]\Big\} p^R_\phi(\phi)\,\mathrm{d}\phi \end{aligned} \tag{61}$$

where $\mathcal{A}$, $\mathcal{B}_c$, and $\mathcal{B}_s$ are the functions defined in (49). Finally, substituting the von Mises PDF $p^R_\phi(\phi)$ into (61), and taking [37, Eq. (3.338-4,)]) into account, we obtain (48).

ACKNOWLEDGMENTS

The authors would like to thank the Associate Editor, Dr. David Matolak, and the anonymous reviewers for their helpful comments and constructive criticism.

This work was financed in part by the Mexican Ministry of Education (SEP) and by the Mexican Council for Science and Technology (CONACYT) through the SEP-CONACYT Basic Research Program: Project references #236188 and #241272.

REFERENCES

[1] D. T. Fokum and V. S. Frost, "A survey on methods for broadband Internet access on trains," *IEEE Commun. Surveys Tuts.*, vol. 12, no. 2, pp. 171–185, Apr. 2010.

[2] G. Araniti, C. Campolo, M. Condoluci, A. Iera, and A. Molinaro, "LTE for vehicular networking: A survey," *IEEE Commun. Mag.*, vol. 51, no. 5, pp. 148–157, May 2013.

[3] A. Osseiran *et al.*, "Scenarios for 5G mobile and wireless communications: The vision of the METIS project," *IEEE Commun. Mag.*, vol. 52, no. 5, pp. 26–35, May 2014.

[4] J. B. Kenney, "Dedicated short-range communications (DSRC) standards in the United States," *Proc. IEEE*, vol. 99, no. 7, pp. 1162–1182, Jul. 2011.

[5] L. Bernado, T. Zemen, F. Tufvesson, A. Molisch, and C. F. Mecklenbräuker, "The (in)validity of the WSSUS assumption in vehicular radio channels," in *Proc. 23rd IEEE International Symposium on Personal, Indoor, and Mobile Radio Communications (PIMRC'12)*, Sydney, Australia, Sep. 2012, pp. 1–6.

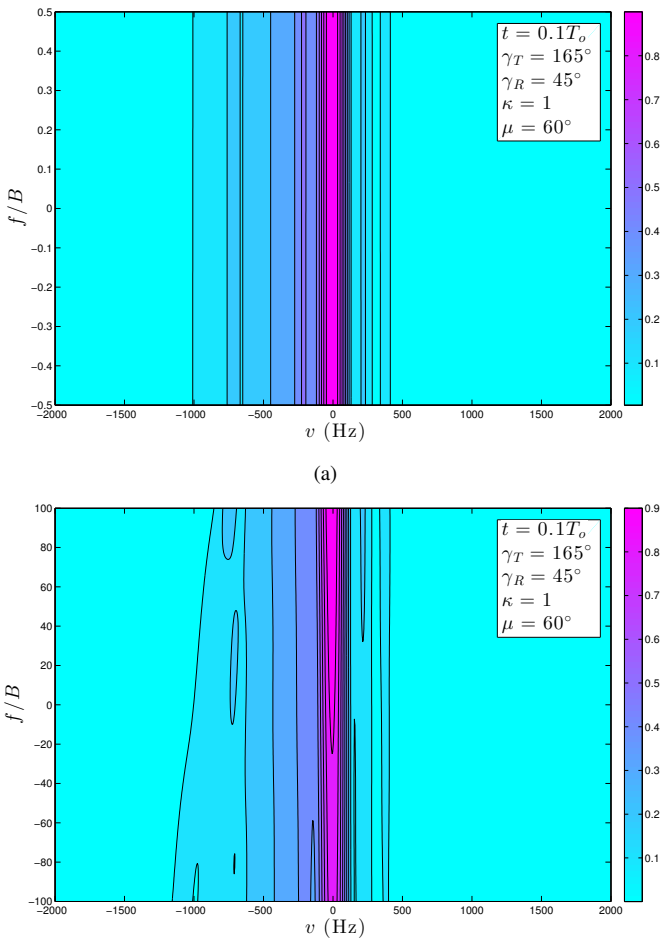

Fig. 12. Color maps of the TF-dependent Doppler profile $\mathcal{D}_H(t, f; v)$ for $t = 0.1\,T_0$, $|v| \leq 2(f^T_{\max} + f^R_{\max})$, and (a) $|f| \leq B/2$, (b) $|f| \leq 100B$.

[6] A. Roivainen, P. Jayasinghe, J. Meinila, V. Hovinen, and M. Latva-aho, "Vehicle-to-vehicle radio channel characterization in urban environment at 2.3 GHz and 5.25 GHz," in *Proc. 2014 IEEE Personal, Indoor, and Mobile Radio Communications (PIMRC'14)*, Washington DC, USA, Sep. 2014, pp. 1–5.

[7] J. Karedal, F. Tufvesson, N. Czink, A. Paier, C. Dumard, T. Zemen, C. Mecklenbräuker, and A. F. Molisch, "A geometry-based stochastic MIMO model for vehicle-to-vehicle communications," *IEEE Trans. Wireless Commun.*, vol. 8, no. 7, pp. 3646–3657, 2009.

[8] F. M. Schubert, M. L. Jakobsen, and B. H. Fleury, "Non-stationary propagation model for scattering volumes with application to the rural LMS channel," *IEEE Trans. Antennas Propag.*, vol. 61, no. 5, pp. 2817–2828, 2013.

[9] M. Walter, D. Shutin, and U.-C. Fiebig, "Delay-dependent Doppler probability density functions for vehicle-to-vehicle scatter channels," *IEEE Trans. Antennas Propag.*, vol. 62, no. 4, pp. 2238–2249, Apr. 2014.

[10] A. G. Zajić, G. L. Stüber, T. G. Pratt, and . T. Nguyen, "Wideband MIMO mobile-to-mobile channels: Geometry-based statistical modeling with experimental verification," *IEEE Trans. Veh. Technol.*, vol. 58, no. 2, pp. 517–534, Feb. 2009.

[11] J. Chen and T. G. Pratt, "A three-dimensional geometry-based statistical model of 2 × 2 dual-polarized MIMO mobile-to-mobile wideband channels," *Modelling and Simulation in Engineering*, vol. 2012, pp. 1–16, 2012.

[12] X. Cheng, Q. Yao, M. Wen, C.-X. Wang, L.-Y. Song, and B.-L. Jiao, "Wideband channel modeling and intercarrier interference cancellation for vehicle-to-vehicle communication systems," *IEEE J. Sel. Areas Commun.*, vol. 31, no. 9, pp. 434–448, Sep. 2013.

[13] A. Abdi and M. Kaveh, "A space-time correlation model for multielement antenna systems in mobile fading channels," *IEEE Trans. Veh. Technol.*, vol. 20, no. 3, pp. 550–560, Apr. 2002.

[14] M. Pätzold, B. O. Hogstad, and N. Youssef, "Modeling, analysis, and simulation of MIMO mobile-to-mobile fading channels," *IEEE Trans. Wireless Commun.*, vol. 7, no. 2, pp. 510–520, Feb. 2008.

[15] C. A. Gutiérrez, J. J. Jaime-Rodríguez, J. M. Luna-Rivera, D. U. Campos-Delgado, and J. Vázquez-Castillo, "Modeling of non-WSSUS double-Rayleigh fading channels for vehicular communications," *Wireless Communications and Mobile Computing*, vol. 2017, pp. 1–13, 2017.

[16] L. Bernado, T. Zemen, F. Tufvesson, A. F. Molisch, and C. F. Mecklenbräuker, "Delay and Doppler spreads of nonstationary vehicular channels for safety-relevant scenarios," *IEEE Trans. Veh. Technol.*, vol. 63, no. 1, pp. 82–93, Jan. 2014.

[17] W. C. Jakes, *Microwave Mobile Communications*. Piscataway, NJ: IEEE Press, 1994.

[18] R. H. Clarke, "A statistical theory of mobile radio reception," *Bell Syst. Tech. J.*, vol. 47, pp. 957–1000, Jul. 1968.

[19] W. L. Stutzman and G. A. Thiele, *Antenna Theory and Design*, 2nd ed. New Jersey: John Wiley and Sons, 1998.

[20] J. G. Proakis, *Digital Communications*, 4th ed. New York: McGraw-Hill, 2001.

[21] F. Bøhagen, P. Orten, and G. E. Øien, "On spherical vs. plane wave modeling of line-of-sight MIMO channels," *IEEE Trans. Commun.*, vol. 57, no. 3, pp. 841–849, May 2009.

[22] C. A. Gutiérrez, M. Pätzold, W. Dahech, and N. Youssef, "A non-WSSUS mobile-to-mobile channel model assuming velocity variations of the mobile stations," in *Proc. 2017 IEEE Wireless Communications and Networking Conference (WCNC'17)*, San Francisco CA, USA, 2017, pp. 1–6.

[23] B. O. Hogstad, C. A. Gutiérrez, M. Pätzold, and P. M. Crespo, "Classes of sum-of-cisoids processes and their statistics for the modelling and simulation of mobile fading channels," *EURASIP Journal on Wireless Communications and Networking*, vol. 2013, no. 2013:125, pp. 1–15, May 2013.

[24] M. Pätzold and B. Talha, "On the statistical properties of sum-of-cisoids-based mobile radio channel simulators," in *Proc. 10th International Symposium on Wireless Personal Multimedia Communications (WPMC'07)*, Jaipur, India, Dec. 2007, pp. 394–400.

[25] J. Jaime-Rodríguez, C. A. Gutiérrez, M. Luna-Rivera, and D. U. Campos-Delgado, "First-order statistics analysis of two new geometrical models for non-WSSUS mobile-to-mobile channels," in *Proc. of the 12th IEEE Int. Conf. on Wireless and Mobile Computing, Networking and Communications (WiMOB 2016)*, New York, USA, Nov. 2016, pp. 1–8.

[26] G. Matz, "On non-WSSUS wireless fading channels," *IEEE Trans. Wireless Commun.*, vol. 4, no. 5, pp. 2465–2478, Sep. 2005.

[27] A. Papoulis and S. U. Pillai, *Probability, Random Variables and Stochastic Processes*, 4th ed. New York: McGraw-Hill, 2002.

[28] R. He, O. Renaudin, K. H. V.-M. Kolmonen, Z. Zong, B. Ai, and C. Oestges, "Characterization of quasi-stationarity regions for vehicle-to-vehicle radio channels," vol. 63, no. 5, pp. 2237–2251, May 2015.

[29] T. J. Willink, "Wide-sense sationarity of mobile MIMO radio channels," *IEEE Trans. Veh. Technol.*, vol. 57, no. 2, pp. 704–714, Mar. 2008.

[30] A. Borhani and M. Pätzold, "Correlation and spectral properties of vehicle-to-vehicle channels in the presence of moving scatterers," *IEEE Trans. Veh. Technol.*, vol. 62, no. 9, pp. 4228 – 4239, Nov. 2013.

[31] W. Dahech, M. Pätzold, C. A. Gutiérrez, and N. Youssef, "A non-stationary mobile-to-mobile channel model allowing for velocity and trajectory variations of the mobile stations," *IEEE Trans. Wireless Commun.*, vol. 16, no. 3, pp. 1987–2000, Mar. 2017.

[32] B. Boashash, *Time Frequency Signal Analysis: A Comprehensive Reference*. Amsterdam: Elsevier, 2003.

[33] L. Cohen, *Time-Frequency Analysis*. New Jersey: Prentice Hall, 1995.

[34] R. von Mises, "Über die 'Ganzzahligkeit' der Atomgewichte und verwandte Fragen," *Physikalische Zeitschrift*, vol. 19, pp. 490–500, 1918.

[35] A. Abdi, J. A. Barger, and M. Kaveh, "A parametric model for the distribution of the angle of arrival and the associated correlation function and power spectrum at the mobile station," *IEEE Trans. Veh. Technol.*, vol. 51, no. 3, pp. 425–434, May 2002.

[36] R. D. Yates and D. J. Goodman, *Probability and Stochastic Processes: A Friendly Introduction for Electrical and Computer Engineers*, 2nd ed. New Jersey: John Wiley and Sons, 2005.

[37] I. S. Gradshteyn and I. M. Ryzhik, *Table of Integrals, Series and Products*, 7th ed. New York: Academic Press, 2007.

Carlos A. Gutiérrez received the B.E. degree in electronics and digital communication systems from Universidad Autónoma de Aguascalientes, Mexico, in 2002; the Advanced Studies Diploma in signal processing and communication theory from Universidad Politécnica de Cataluña, Spain, in 2005; the M.S. degree in electronics and telecommunications from CICESE, Mexico, in 2006; and the Ph.D. degree in mobile communication systems from the University of Agder, Norway, in 2009. From 2009 to 2011, he was with the School of Engineering, Universidad Panamericana Campus Aguascalientes, Mexico. Since January 2012, he has been with the Faculty of Science, Universidad Autónoma de San Luis Potosí, Mexico. His research interests include modeling and simulation of mobile fading channels for wireless communication systems, and physical layer aspects of OFDM and MC-CDMA systems. Dr. Gutierrez has served as a Guest Editor for the journals *Wireless Communications and Mobile Computing*, *Modelling and Simulation in Engineering*, *Procedia Technology*, and *Research in Computing Science*, and as technical program committee member for various international conferences. He is a member of the Mexican National System of Researchers (SNI).

José T. Gutiérrez-Mena received the B.S. and M.Eng. degrees in electronics engineering from the Autonomous University of San Luis Potosi, Mexico, in 2012 and 2014, respectively. He is currently a Ph.D. student at the Faculty of Science, Autonomous University of San Luis Potosi. His current research interests include V2V communications, channel modeling, MIMO systems, and non-stationary channels..

José M. Luna-Rivera received the B.S. and M.Eng. in electronics engineering from the Autonomous University of San Luis Potosi, Mexico, in 1997 and 1998, respectively. He received the Ph.D. degree in electrical engineering from the University of Edinburgh, UK, in 2003. He is currently an Associate Professor at the College of Sciences of the Autonomous University of San Luis Potosi, Mexico. His research focuses on signal processing for wireless communication and visible light communications.

Daniel U. Campos-Delgado was born in San Luis Potosi, Mexico, on October 14, 1973. He received the B.S. in electronics engineering from the Autonomous University of San Luis Potosi, Mexico, in 1996, the M.S.E.E. and the Ph.D. degrees from Louisiana State University in 1999 and 2001, respectively. In May 2001, the College of Engineering of LSU granted him the "Exemplary Dissertation Award", and in 2009, he received the "University Award for Technological and Scientific Research" as a Young Researcher from the Autonomous University of San Luis Potosi. In 2001, he joined the College of Sciences of the Autonomous University of San Luis Potosi as a professor. He has published more than 150 referred papers in scientific journals and congresses. His research interests include power control in wireless systems, optimization, dynamic modelling and optimal signal processing.

Ramiro Velázquez received the PhD in Robotics from Université Pierre et Marie Curie – Paris 6 (France) in 2006. Since 2006, he is an Associate Professor at Universidad Panamericana (Mexico). He is past Dean of the Faculty of Engineering and currently serves as Vice-President for Research. He is considered an expert evaluator for the European Commission, CONACYT (Mexico), and COLCIENCIAS (Colombia). He is a member of the Mexican National Systems of Researchers (SNI). His current research interests are assistive technologies and mechatronic systems.

Matthias Pätzold (M'94SM'98) received the Dipl.Ing. and Dr.-Ing. degrees in electrical engineering from Ruhr-University Bochum, Bochum, Germany, in 1985 and 1989, respectively, and the Habiliation degree in communications engineering from the Technical University of Hamburg, Harburg, Germany, in 1998. From 1990 to 1992, he was with ANT Nachrichtentechnik GmbH, Backnang, Germany, where he was involved in digital satellite communications. From 1992 to 2001, he was with the Department of Digital Networks, Technical University of Hamburg. Since 2001, he has been a Full Professor of mobile communications with the University of Agder, Grimstad, Norway. He has authored several books and numerous technical papers. His publications received 13 best paper awards. He has been actively participating in numerous conferences, serving as a member and the chair of technical program committees. He is currently an Associate Editor of the *IEEE Vehicular Technology Magazine*.